A multispectral imaging method and device to detect and quantify the presence of fluid in the middle ear to facilitate the diagnosis and triage of ear infections.

by
Gokul Prasath Rajamanickam

B.E. Biomedical Engineering
PSG College of Technology (India) 2012

SUBMITTED TO THE SYSTEM DESIGN AND MANAGEMENT PROGRAM
IN PARTIAL FULFILMENT OF THE REQUIREMENTS FOR THE DEGREE OF

MASTER OF SCIENCE IN ENGINEERING AND MANAGEMENT
AT THE
MASSACHUSETTS INSTITUTE OF TECHNOLOGY

MAY 2020

Signature of Author: _____
Gokul Prasath Rajamanickam
System Design and Management Program
May 08, 2020

Certified By: _____
Nevan C. Hanumara
Research Scientist, Mechanical Engineering
Thesis Supervisor

Certified By: _____
Nicholas X. Fang
Professor, Mechanical Engineering
Thesis Supervisor

Accepted By: _____
Joan S. Rubin
Executive Director, System Design and Management

[This page is intentionally left blank.]

A multispectral imaging method and device to detect and quantify the presence of fluid in the middle ear to facilitate the diagnosis and triage of ear infections.

by
Gokul Prasath Rajamanickam

Submitted to the System Design and Management Program in May 2020
In Partial Fulfilment of the Requirements for the Degree of
Master of Science in Engineering and Management

Abstract

Middle ear infections or otitis media that cause inflammation of tympanic membrane and fluid buildup in the middle ear cavity accounts for 2-3 million hospital visits every year [34]. As per an epidemiological study conducted from 2006 - 2016 on 685 children, between the ages of 1-3 years, roughly 60% had at least one hospital visit due to ear infections [3]. Despite the high incidence, the diagnosis of otitis media is only 50% accurate (a coin toss) due to the subjective nature of diagnosis as the physicians look at the ear drum and detect the fluid behind the ear drum. To detect the fluid with high sensitivity and accurately diagnose middle ear infection, we propose a multispectral visible – nIR otoscope that operates in the range of 600 nm – 1050 nm. We have performed experiments to demonstrate the proof of concept of our device on phantoms that includes, 3D printed middle ear structure, tympanic membrane made of silicone, and orange juice as ear fluid all of which mimics the properties of human ear. The multispectral otoscope showed highest contrast between ossicles and fluid at 1000 nm which shows low attenuation of fluid and tympanic membrane at NIR wavelengths. The system is calibrated against a diffuse reflection surface to account for variations in source and detector. Our experiments showed that empty phantoms yielded almost equal contrast across the entire visible- NIR wavelength. Once the fluid is filled, the contrast increased by 30 ± 10 % in the visible wavelength (600 nm - 750 nm) and 120 ± 20 % in nIR wavelength (900 nm – 1000 nm). This 80% - 100% difference in contrast between visible and NIR wavelength is used to detect and highlight the areas of the middle ear filled with fluid.

Thesis Supervisor: Nevan C. Hanumara
Title: Research Scientist, Mechanical Engineering

Thesis Supervisor: Nicholas X. Fang
Title: Professor of Mechanical Engineering

[This page is intentionally left blank.]

Acknowledgments

This work was made possible by the collaboration and support of many talented individuals.

Firstly, I want to thank the entire staff and faculty of the system design and management program for providing me a chance to learn at this world-class institution, and supporting my academic and career interest throughout these past two years.

Next, I would like to express my deep gratitude to my thesis advisor and mentor Dr. Nevan Clancy Hanumara for providing all possible support over the past year and bringing this project to fruition. I would also like to thank him for providing guidance and support for my career and personal endeavors. I want to profoundly thank Dr. Nicholas Xuanlai Fang for being my advisor and providing me with the technical guidance and infrastructure needed to finish this work. I would like to thank all the members of Fang lab for providing me valuable suggestions. I would especially like to thank Xinhao Li for his valuable suggestions and technical insights on optics throughout this project.

I would like to thank Dr. Dennis Poe and Dr. George Kenney for finding this need, proposing this project to MIT 2.75 Medical device design class, and providing their clinical expertise and inputs throughout the project. This thesis work was made possible by Jack Erdozain Jr. and myself as we conceived the multispectral imaging idea along with the excellent contributions from Hope Chen and Dominic Martinez. I would like to acknowledge the efforts of entire 2.75 course staff for guiding us through the product development. I would also like to thank Dr. Jana M. Kainerstorfer, Assistant professor of Biomedical engineering at CMU for her valuable inputs on optics.

I am thankful to the Department of Mechanical Engineering for providing the Teaching Assistantship over the last two years. I am especially grateful to Dr. Barbara Hughey for believing in me and encouraging me to teach the course 2.671, which enriched my knowledge of the subject and provided me with a great teaching experience. I would like to thank all my friends and colleagues at the MIT SDM program, MIT Sloan Healthcare Club and the rest of MIT and MIT Sloan, for providing an inclusive learning environment over the last two years.

I would also like to thank my previous employers and colleagues at Achira Labs, India, and at Technology Strategy Partners (TSP), Cambridge, MA, for all the learnings and experience that led me here. I am grateful to Dr. Bruce Cameron, Partner at TSP, for guiding and helping me navigate my academics and career. I would like to convey my profound gratitude to my mentor Dr. Dhananjaya Dendukuri, CEO, Achira Labs, for being a source of inspiration and encouraging me to follow my dreams.

I am indebted to all my professors from the Department of Biomedical Engineering, PSG College of Technology, India, and the Department of Electronics and Communications Engineering, PSG Polytechnic College, India, for giving me a robust technical foundation and

instilling strong ethics. I am especially thankful to Dr. Lakshmi Deepika, Ms. Lakshmi Prabha, Mr. Vignnesh Babu, and Mr. Murali Krishnan for having a positive impact and helping to shape my early learnings and career.

I am grateful to all my friends from home in India for their support. A special mention to Shanthanu Sethupathi for being my pillar of support over the last decade, my friend and roommate Gauthaam Sarathy for tolerating me, and motivating me to aspire higher. I would like to give a special mention to my friend and mentor, Sendil Kumar, for all the run-and-learn lessons, and providing me with the constant support and encouragement that made my MIT dream possible. Last, but not the least, I would like to convey my heartfelt thanks to my family; my mother - Thirumathal Rajamanickam, and my father – Rajamanickam Kumarasamy, for always providing me with more than what I need and fulfilling my higher education dream; my uncle – Gnanasekar, my sister – Gayathri Rajamanickam, and my lovely fiancé - Vijetha Prakash, for always believing in me and giving me all the support I needed, all of which helped me successfully complete this degree.

[This page is intentionally left blank.]

Table of Contents

List of Figures

List of Tables

[This page is intentionally left blank.]

Chapter 1 | Introduction

"நோய்நாடி நோய்முதல் நாடி அதுதணிக்கும்
வாய்நாடி வாய்ப்பச் செயல்"

- Thiruvalluvar (31 BCE, written in the Tamil Language)

Translation:
Let the physician inquire into the (nature of the) disease, its cause and its method of cure and treat it faithfully according to (medical rule).

Accurate medical diagnosis is essential to understand the disease condition, decide the course of treatment and predict disease outcomes. Medical diagnosis had evolved from simple empirical rules, observing physical symptoms, using microscopes to look at the blood cells, imaging to look at various organs, using proteins and other blood components to diagnose a disorder, and the use of genetic markers to not only diagnose complex diseases, such as cancer, but also identify at risk individuals. But the evolution of diagnostic technologies has not evenly impacted all diseases with many common, treatable diseases still diagnosed empirically. This is especially the case with the diagnosis of middle ear infections. Middle ear infections or otitis media cause inflammation of tympanic membrane and surrounding tissues and leads to fluid buildup in the middle ear cavity, which is otherwise an air-filled space.

1.1|Research Motivation

As per an epidemiological study conducted from 2006 - 2016 on 685 children, between the age of 1-3 years, roughly 60% had at least one hospital visit due to ear infections [3]. Otitis media is diagnosed when there is an inflammation of the Tympanic Membrane (TM) and fluid is present behind the TM. Ear infection can be primarily classified into two categories namely Acute Otitis Media (AOM) and Otitis Media with Effusion (OME). Some of the common tools to diagnose infection include video otoscope, pneumatic otoscope, and tympanometry.

Based on the diagnosis of AOM or OME, a physician can decide to wait until infection resolves by itself, prescribe antibiotics, or conduct a surgical intervention. But these decisions are typically made without accurate information pertaining to the presence or absence of the fluid in the middle ear, except in cases of rupture of tympanic membrane. As per a recent study [31], 80-90% of general physicians and specialists use an otoscope for diagnosis although these do

not provide accurate information needed for diagnosis. Several studies [30,32] have found that diagnostic accuracy of AOM varies widely among physicians and at present 50% of cases are overly diagnosed as AOM, when it should have been OME. The AAP [2] recommended the limited the use of antibiotics but the improper diagnosis leads to physicians prescribing antibiotics for treating the infection. It is widely known that anti-microbial resistance is turning into a global public health issue and a study [29] found that use of antibiotics to treat childhood ear infections has been linked to increasing antibiotic resistance. The primary issue preventing physicians and researchers from obtaining accurate information about AOM is unavailability to diagnostic tools.

AOM has various stages of severity based on ear pathology and physiological signs [2] and, according to a report from the American Academy of Pediatrics, an estimated 8 million children are affected by AOM in the US annually [4], as shown in Figure 1.1. Once diagnosed, children are treated with antibiotics, often more than once before the infection is cured.

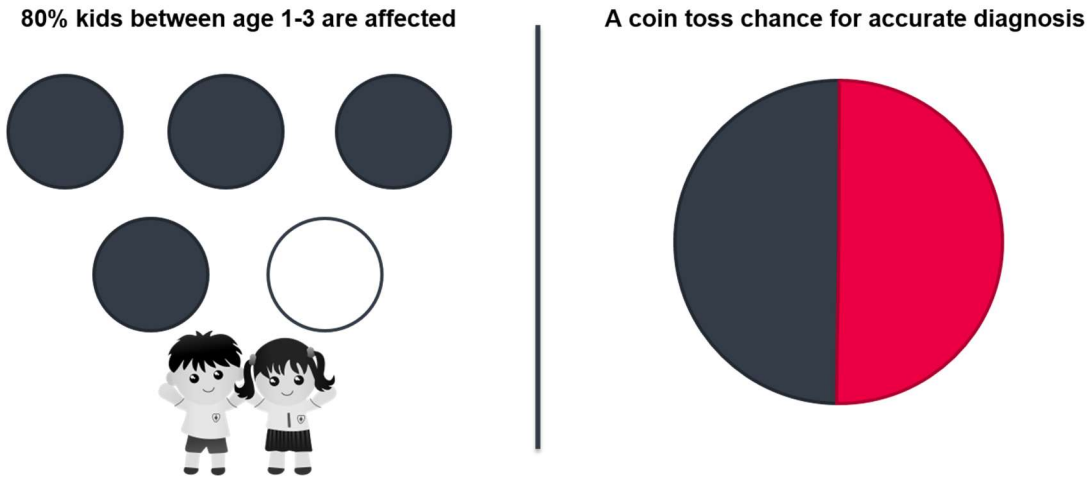

Figure 1.1 Diagnostic Accuracy and Infection rate

AOM often presents with Tympanic Membrane or Ear drum inflammation and a cloudy, puss-like middle ear fluid behind the membrane and patients develop these symptoms suddenly and may have a high fever, earache, and respiratory disorders. OME has very similar ear pathology to AOM, with the only distinction being the absence of acute symptoms. Unlike AOM, which occurs due to anaerobic bacterial infections, OME can occur due to a blocked Eustachian tube, often during a respiratory illness, or as an aftermath of AOM. OME may resolve itself over time or be cured using tympanocentesis (draining the middle ear fluid) unlike AOM, which needs

to be treated with antibiotics. In contrast, OME should not be treated with antibiotics as mentioned earlier.

A typical clinical exam consists of checking overall symptoms and visual observation of the ear drum via otoscope, where the physician looks for bulging, redness and the presence of liquid behind the ear drum. Without a means to quantify the presence of fluid in the middle ear, as shown in Figure 1.1 right, this exam is has no better accuracy than a coin toss as a differentiator between AOM and EOM.

This thesis presents a handheld, multispectral imaging otoscope which provides physicians and researchers, an objective and quantitative way of detecting the presence or absence of fluid in the middle ear, a diagnosis currently done subjectively.

1.2|Stakeholder & Market Analysis

A key step in developing any new technology is a stakeholder analysis to identify the parties that influence the design and deployment.

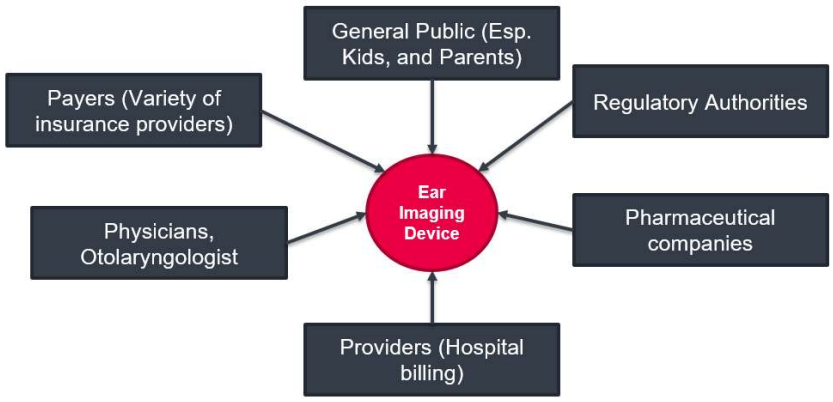

Figure 1.2 Stakeholder network for an Ear Imaging Device

Figure 1.2 identifies the main stakeholders common to any new medical device. This work proposes a device for in clinic-use based on an otoscope, a relatively simple, durable tool used by otolaryngologists and ENT specialists, as well as general physicians. Unlike more sophisticated medical devices, otoscope use is not covered under any procedural or diagnostic reimbursement code, therefore, payers will have little immediate influence on adoption.

Physicians, in conjunction with their facilities (providers), will be the biggest influencers. Facilities buy otoscopes as capital equipment along with single-use specula and the cost of

purchase and minimal maintenance must be amortized across multiple patient visits. The proposed device's use will have to be justified to providers in terms of better patient care and decreased costs to their practices. Later, pending studies showing that patient outcomes are improved and, ideally, costs are reduced as a result of more accurate diagnoses and treatments, a case could be made for reimbursement, whereupon the payers will become important stakeholders. Therefore, minimizing cost is an important design requirement to keep the cost of device (capital equipment) as low as possible.

Parents, shown in Figure 1.3, are stakeholders who do not influence the functional performance of the device, since they are not the final authority in the diagnosis of the infection, but they may influence clinicians' purchase decisions if they perceive that the technology is providing a better level of care.

Other opportunities exist for the device proposed herein. Over the last few years, there has been a growing interest in self-diagnosis and remote diagnosis, with the advent of tools for telemedicine. The different models of otoscope that are being sold in large numbers in Amazon is a testament to parents' interest in owning an otoscope device to perform at-home testing before visiting a doctor.

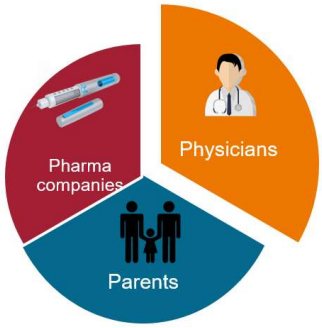

Figure 1.3 Market Segmentation

Also shown in Figure 1.3, pharmaceutical companies may, potentially, be incentivized to support a technology that more decisively determines when prescriptions antibiotics are needed. Furthermore, recent advancements in regenerative medicine led companies to develop therapies to treat Sensory Neuronal Hearing Loss (SNL) [20]. SNL is associated with 90% of hearing loss due to aging, birth defects, and accidents. The therapeutic drug needs to be delivered in the inner ear to regenerate the lost hair cells and this advancement provides a potential opportunity for an

imaging device to see through the TM to aid in delivery. If an improved otoscope-like device can be used as a dedicated tool for therapeutic delivery, then payers and pharmaceutical companies will play a role in creating a new use case for this device and a new reimbursement model that could increase the value of the device. Although the regulatory pathway is complicated, a 510(k) clearance can be sought for both use cases since otoscope devices are standard, and there has been plenty of drug delivery devices in the market.

1.3|Disease state fundamentals

The American Academy of Pediatrics has a standard guideline [2] to diagnose ear infections and classify them, with the most commonly diagnosed being Acute Otitis Media (AOM) and Otitis Media with Effusion (OME), with more details in Table 1.1.

To better understand the disease fundamentals of otitis media, it is important to discuss ear anatomy and specific disease states. The ear is typically segmented it into three parts, as shown in Figure 1.4, namely, the outer ear, middle ear, and inner ear.

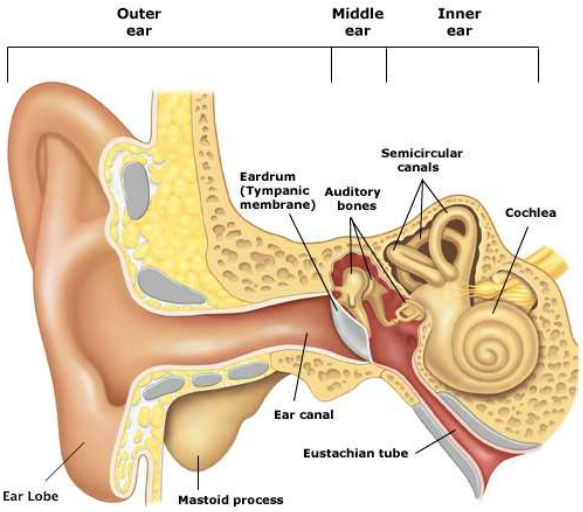

Figure 1.4 Anatomy of Middle ear, source: earnosethroat.com.au

The outer ear consists of the ear lobe and ear canal, both of which are not affected by ear infections, but provide an opening to examine the infection. The middle ear consists of the Tympanic Membrane, Incus, Malleus, and Eustachian tube. The inner ear consists of three semi-circular canals, which are tiny fluid-filled tubes that help maintain orientation, and the Cochlea, the spiral cavity of the inner ear containing the organ of Corti, which produces nerve impulses in

response to sound vibrations. Even though the inner ear is not directly affected by infection, the auditory bones (incus, malleus, stapes) will not receive the auditory signals and can lead to conductive hearing loss in some cases.

Middle ear infections can be caused by bacterial or viral infections resulting from illnesses including the common cold, flu, or allergies. These common illnesses can also lead to congestion and blockage of nasal passages, throat, and Eustachian tubes. The blockage combined with the infection leads to fluid buildup in the middle ear, pressure and discomfort. As shown in Figure 1.4, the Eustachian tubes are a pair of narrow tubes that run from the middle ear to in the back of the throat, behind the nasal passages. These regulate air pressure exchange air, and drain normal secretions from the middle ear [1]. Once the Eustachian tubes become blocked due to illness, fluid secretions stay in the middle ear, leading to infection and the onset of symptoms such as ear pain, swimmers ear, a twitching or pulling sensation in the ear, and temporary loss of hearing. Children are especially at risk of ear infections since their Eustachian tubes are narrower and more horizontal and thus more easily blocked. Ear infections can be both acute and chronic, with multiple stages and Table 1.1 summarizes the common types of infections, symptoms, pathology, diagnosis and treatment.

Table 1.1 Types of Middle ear infection

Type of infection	Disease state, Symptoms, and Diagnosis
Acute Otitis Media (AOM)	Acute Otitis Media is caused by a viral or bacterial infection. The Tympanic Membrane appears red and inflamed with a thick puss like fluid behind the membrane. The fluid is not directly observable unless there is a rupture of the membrane in which case the fluid / puss drips out of the middle ear. AOM is often accompanied by severe ear pain, headache, and fever. As per the guideline issued by American Academy of Pediatrics, an AOM diagnosis requires either moderate to severe bulging of the TM, a new onset of otorrhea (discharge from not caused by otitis externa or an ear canal infection) mild bulging of the TM associated with recent onset

	of ear pain (less than 48 hours), or erythema (inflammation) [2]. Diagnosis is by symptoms and direct observation. AOM is normally treated with prescription antibiotics. AOM should not be diagnosed in children who do not have objective evidence of OME.
Otitis Media with Effusion (OME)	Fluid effusion continues to present in the middle ear even after the initial infection is reduced. OME can also occur without ever having an acute infection. OME can also be caused by cold which leads to closing of Eustachian tubes and nasal pathways. OME may cause a feeling of fullness in the ear, lead to temporary loss of hearing or remain asymptomatic. Similar to AOM, OME is primarily diagnosed by looking at the TM. A retracted or less/non-inflamed TM, with the presence of ear fluid behind the membrane, is an indication of OME. Diagnosis is by symptoms and direct observation of the TM and, as per the American Association of Pediatrics [2] this condition should not be treated with antibiotics and the patient should be observed and the condition allowed to resolve.
Chronic Otitis Media with Effusion (COME)	Fluid remains in the ear for a prolonged time either with or without an infection and this can occur repetitively even after multiple treatments. The presence of fluid over long periods dampens the sound transfer from the TM to the auditory bones, which may lead to difficulty in fighting new infections and ultimately hearing loss. Diagnosis is by looking at the tympanic membrane for the fluid behind the membrane. Treatment involves the surgical placement of a drainage tube through the TM to relieve pressure, enable drainage and ventilate the middle ear. The entry of oxygen into the middle ear which prevents anaerobic bacterial infection. The tube is retained for 3-6 months and usually falls out as the TM repairs itself and pushes the tube out.

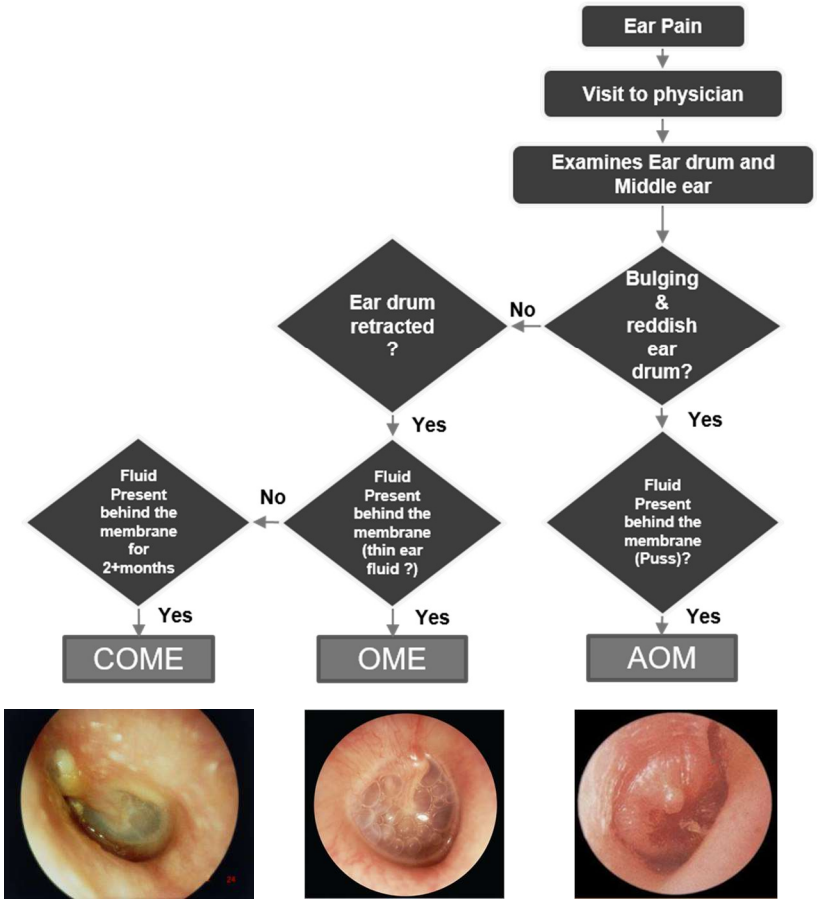

[37] [36] [38]

Figure 1.5 Ear infection diagnosis flow chart

Figure 1.5 details the diagnostic criterion when a child is suspected of having an ear infection, based on observation with a video otoscope and/or a pneumatic otoscope. The otoscopes help to look at the changes in tympanic membrane, but the presence of fluid behind the membrane is subjectively determined by the physician. The Pneumatic otoscope helps the physicians to observe the vibrations in the tympanic membrane by introducing a positive air pressure in the ear canal. It is important to note that both the cases above are subjective to the interpretation of the physician and can vary widely as noted in various studies [30,32]. The fluid presence can absolutely be determined only in the case of an infection severe enough to cause rupture of the TM.

1.4|Research Statement

To address the need for better inner ear diagnostic information, this this work proposes a system to:

To: diagnose and quantify the fluid present in the middle ear

By: imaging the TM and the middle ear structures

Using: multispectral source and an imaging system

While: Exploiting the spectral properties of the TM and ear fluid

The core of this research involves identifying suitable wavelength(s) in the visible and nIR region that can be used to detect the fluid behind the membrane with high sensitivity which in turn provides a method to diagnose middle ear infections. The research focuses on creating a low-cost, handheld device that is physically very similar to the existing otoscopes, but provides functional improvements to quantitatively detect fluid behind the tympanic membrane thereby providing physicians an objective and sensitive tool for ear infection diagnosis.

1.5|Thesis Overview

Chapter 2

This chapter reviews existing literature to understand the evolution of technologies for otitis media infection diagnosis.

Chapter 3

This chapter presents middle ear biological tissue properties, the phantoms which are used for testing, applicable multispectral physics theory, and device architecture.

Chapter 4

This chapter discusses the system calibration, qualitative and quantitative data analysis under various experiment conditions, summarizes the key results.

Chapter 5

This chapter provides conclusions, and recommendations for future work

Chapter 2 | Literature Review: Devices for Diagnosing Ear Infection

The earliest known history of a tool to diagnose ear and nose infections was envisioned by a French physician and surgeon named Guy de Chauliac in 1364 [6] but the proposed 'Otoscope' was not created until the 1600's and 1700's when a German physician Wilhelm Fabry, and a medical device salesman J.J Perret created the first working prototypes. Thus, Otoscopes came into widespread use in the middle of the 17th century. Throughout the 18th and 19th century, many researchers continued to make incremental improvements. Modern day devices include an opening to introduce positive air pressure into the ear cavity and observe the vibrations of the TM (Pneumatic Otoscope) was invented by another German physician, E. Siegle in 1864 [6]. The otoscope in its current form with bell shaped speculum was invented by A Hartman in Germany, 1880. A brief history of all ear imaging modalities is given in a timeline in Figure 2.1 below.

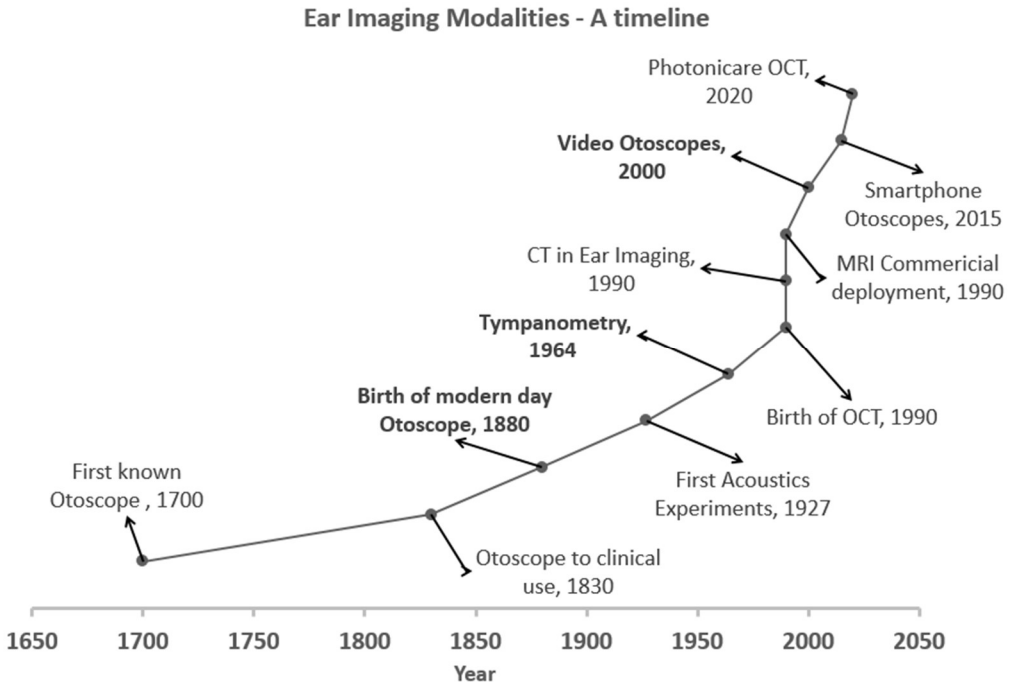

Figure 2.1 A Timeline showing commercially available ear imaging modalities. Inventions shown in bold are the ones which provided big improvements in otitis media diagnosis

As shown in Figure 2.1above, much of the improvements in ear imaging technology happened in the last four decades due to the technological advancements in silicon detectors, optical lenses, and light sources. During this time, improvements in otoscopes have largely been incremental, including: improving the lenses to reduce aberration and increase magnification to view the entire tympanic membrane, providing manual magnification option, adding low-cost and high intensity light sources like LEDs, and adding cameras for capturing the images. Although non-invasive imaging technologies, including Optical Coherence Tomography and Ultrasound, have come into widespread use for medical imaging, the acceptance of such techniques in the ENT specialty has been very low due to high costs and the resulting devices' bulky nature. Doctors still prefer to use an otoscope, due to cost, availability, training, and ease of use [31]. Despite low acceptance, the biomedical research community has worked extensively on improving ear imaging technologies in the last two decades. This chapter discusses about many such promising technologies which are in various stages of commercialization.

2.1|Commercially available devices

As mentioned earlier, an otoscope is a commonly used device for examining the ear, nose, and throat. The ear speculum it typically disposable and attaches to the proximal end of the device, as shown in Figure 2.2 (a). This is available in different lengths and diameters to accommodate everyone from infants to seniors and provide different field of views.

(a) (b) (c)

Figure 2.2 Otoscope and its variations

The handle usually contains a battery to provide power to the light source, which is placed right at the entrance of the speculum. The eyepiece consists of a convex lens that focuses the light

from the TM. The otoscope shown in Figure 2.2 (a) is a simple and low-cost device, typical of that used by most physicians. The otoscopes in Figure 2.2 (b) and (c) are modifications that allow physicians to view the image on a computer screen or on an LCD attached to the device respectively. The image quality in these devices depends highly on the cameras and displays.

All clinical otoscopes come with an add-on for attaching a balloon pressure handle, to momentarily introduce a positive air pressure in the middle ear cavity. This type of device, called a pneumatic otoscope, provides additional information by enabling a clinician to generate and observe the vibrations of the TM. Oscillations are dampened when the liquid is present in the middle ear, so this helps identify when the middle ear is filled, but still requires subjective interpretation.

When otoscopic examination does not provide conclusive evidence to diagnose the type of ear infection or doctors want to check for long-term problems they may perform one of the following additional procedures for supplemental information: 1) Tympanometry 2) Acoustic Reflectometry and 3) Tympanocentesis.

Tympanometry objectively measures the energy transmission through middle ear by measuring the sound reflected from tympanic membrane under different air pressures. Tympanometry is performed by sealing off the ear canal, adjusting the air pressure to a known value, and introducing a 200 Hz – 2 kHz audio signal in the middle ear canal. The reflected sound is plotted against air pressure called tympanogram. A normal, a bulging ear drum with fluid buildup, and a retracted ear drum produces different tympanograms (resulting waveform shapes resembles that of the tympanic membrane shape). This can identify the presence of liquid by proxy measurement of pressure in the middle ear. As mentioned earlier, this can only be used in conjunction with standard otoscope to supplement information, but not as an independent diagnostic device.

Acoustic Reflectometry measures the amount of sound reflected from the TM and provides a qualitative measure of the middle ear effusion. This is performed by doing a sound sweep on a large frequency spectrum and measuring the reflected signal. Unlike tympanometry, there is no need to seal the ear canal and this test can be easily performed in the bed side. In normal cases, the TM transmits the sound waves' energy to the inner ear via the auditory bones

and therefore lesser sound is reflected back. But when there is pressure and fluid buildup in the middle ear, it attenuates the sound transmission into the bones and more sound is reflected, confirming the presence of fluid. However, most measurements are relative as there are no established standards to interpret the reflectometry results between normal and ears with middle ear effusion.

Tympanocentesis is a mini surgical procedure performed on patients who have chronic otitis media with effusion (COME). The physician makes a small puncture to drain the fluid. In extreme cases, large incisions have to be made to avoid blockages and the fluid drains in large quantity. Often a tiny tube placed to facilitate continue drainage. This typically falls out on its own once the condition resolves and the membrane heals.

2.2|Technologies under development

The following section describes various technologies that are currently under development. Using the information available, each of the technologies has been classified under NASA Technology Readiness Level (TRL) guidelines [7] to compare all the technologies on a standard scale and to provide a sense of how far along these technologies are on the road to commercialization. The technologies that are *starred in the table refers to those that directly address otitis media diagnosis.

Table 2.1 List of Competing Technologies

Description	Analysis	TRL
***SWIR Otoscope:** Short Wave Infrared Imaging (SWIR) takes advantage of the lower scattering properties of infrared light at higher wavelengths to visualize structures behind the translucent TM. (In the visible light range diseased membranes can have widely varying and higher diffraction due to structural and biological changes.) But such conditions	The technology provides low resolution, but high sensitive and quantitative detection of middle ear fluid. An important advantage is that it removes the attenuation effects of the TM from the imaging equation and the final device and operating procedures resembles that of standard video otoscope. A disadvantage of SWIR is that it requires specially made optical components and non-	7

do not affect the transmission of light at NIR and IR wavelengths. SWIR uses every high attenuation of ear fluid and low attenuation from the tympanic membrane at about ~1400 nm to differentiate fluid and diagnose middle ear infections. [8].	silicon detectors (cameras). The SWIR cameras are very expensive due to limited scale and restricted by ITAR. This makes commercialization difficult on a global scale.	
Otoscopy and Spectroscopy: This technology is in its early research stage and proposes combining traditional otoscopy with diffuse reflectance spectroscopy and Gas in Scattering Media Absorption Spectroscopy (GASMAS) as a way to diagnosis otitis media. The diffuse reflectance spectroscopy quantitatively measures the change in Hemoglobin content in the TM when it is infected, based on the hemoglobin absorption peaks at 420 and 540 nm. GASMAS helps in determining when the air (gas) has been replaced by fluid [9].	Although this technique leverages peaks, there is no evidence presented as to the magnitude of absorption change in the case of infected persons. The GASMAS measurements were made at 760 nm with a box as a phantom and the change in spectral absorbance between air and water was demonstrated, however, the phantom did not replicate the properties of the TM and middle ear fluid. The data is insufficient to evaluate this technique and the instrumentation presented for two measurement modalities suggests that this may be complicated for the physicians.	1-2
Light Field Otoscope: The system provides a 3D color images of various otitis media conditions [10,11]. It employs a plenoptic camera that has a series of micro lens positioned before the image plane that measure light intensities from each field at different depths. The micro lens helps to capture the light rays traveling in a different direction from each point in the	This is the first system that provides real 3D images of the TM and quantifies the bulging or retraction. This is better than a qualitative examination of the TM with a normal otoscope. The device falls short of diagnosing the presence of fluid, which was not in the scope of work. Although doctors look for changes in TM, the accurate diagnosis can only be made in conjunction	4-5

object plane, thus providing an option to capture a depth object with different focus at each point. The image is then passed through an algorithm to extract multiple views and compute the 3-dimensional view of the TM namely superior, anterior and ventral view. The clinical data shows decent accuracy which can classify TM bulging or retraction when it is more than +/- 2 mm. [11].	with the information on the presence or absence of fluid. The authors mention the use of broadband 450 nm - 850 nm light source due to the unavailability of other light sources but don't provide any other reasons for the use of a multispectral source.	
***Multicolor Reflectance Imaging:** The otoscope is repurposed to include a multicolor source with red (625 nm), blue (455 nm), and green (523 nm) wavelengths and the images are captured using a video camera. The system uses a filter wheel to create a narrowband source from the wideband incoherent LED sources. The multicolor reflectance imaging uses the absorption properties of TM tissues and blood vessels to provide increased contrast differences between various middle ear structures. The system also uses multiplexed illumination to highlight areas of interest such as lesions, promontories, etc. [12]	The authors argue that a multispectral imaging source can help in identifying different structures, due to tissues' varying scattering properties, however no evidence is presented to explain the selection of the three wavelengths. Some combination of sources do highlight structures, with the help of a contrast limited adaptive histogram equalization technique. The blue and green images, show some qualitative differences in areas with purulent material, however, this still requires subjective interpretation. Additionally, the number of test subjects is not specified, so it not possible to effectively evaluate the spectral response across different subjects.	4
Multiwavelength fluorescence Otoscope: The system uses the auto fluorescent properties of the tissues to diagnose	This is a novel concept that has advantages over all the other multispectral imaging concepts, with the primary being removing	4-5

lesions and infections. The fluorescence measurements are done at wavelengths 405 nm and 450 nm. The device is an extension of the multicolor reflectance imaging otoscope described above, with the addition of high pass emission filters that serve to filter reflected light from the TM and capture auto-fluorescence from the endogenous tissue chromophores, such as collagen, elastin, reduced Nicotinamide adenine dinucleotide (NADH), Formate Dehydrogenase (FDH) [13].	the TM's reflections from the imaging system. The selected excitation wavelengths also have better excitation peaks with respect to the chromophores present in the endogenous tissues. But it's not clear whether the auto-fluorescence signals are coming from a single source/ tissue or a combination of tissues. The device has been tested on 11 patients and the results are promising towards the diagnosis of congenital cholesteatoma. The removal of the TM and the ear fluid from the resulting image to detect the cholesteatoma nullify its use for the detection of otitis media.	
EarID: This otoscope used structured light to obtain a three-dimensional image of the TM. The device excited the TM with five different fringe patterns using a projector and captures the reflected light from the TM using a telecentric optical system and an HD camera. A magnified, 3D surface image of the TM surface was generated using a phase-shifting algorithm [14].	The device uses a similar premise as described in Light Field Otoscope [11] to visualize the 3D structures of the TM, and to aid in otitis media diagnosis. However, the images that are produced from this device looks like computer generated or 3D rendering of the middle ear, not direct visualizations. Moreover, the device only provides indirect depth information in "phase units." Although the idea is novel, extending this beyond the laboratory will be challenging due to complex calibration procedures and would require changes in the current standard of practice.	2

***Spectrometric Otoscope (Oto-Spectroscope):** This is a retrofitted device whereby a scientific spectrometer is fitted inside a traditional otoscope to measure the properties of the middle ear under various otitis media conditions. Specifically, it uses wideband (VIS-NIR) reflectance and scans the ear from 550 nm to 1000 nm. Reflectance patterns are used to determine the presence of liquid and classify between AOM and OME. The reflectance properties of AOM, OME, and normal ear shows a similar bell curve pattern, but different reflectance values [16].	This device was tested in double-blind control studies with 258 patients where both diseased and contralateral images were taken. The results also showed high absorption at 580 nm and 970 nm, and low absorption at 750 nm, but the authors don't discuss whether those differences are statistically significant. The primary disadvantage of the system is not being able to produce multispectral image for analysis. The system collects wideband reflectance spectra from the tympanic membrane, but the data analysis is still very scientific and involves expertise. The physicians might not be able to interpret reflectance spectra and relate it to otitis media diagnosis. The device has scope for further development, but we did not find any follow up work.	3
***Photonicare TOMI Scope:** This packages a portable OCT imaging system with a handheld scanner and it is used to non-invasively and quantitatively measure the TM and biofilm thickness. This quantification of TM thickness is used to diagnose otitis media. The system used a broadband LED source, which has a center wavelength around 840 nm, and the cross-sectional images are processed and the resulting images and thickness of the	Though OCT imaging has been used for otitis media diagnosis, it was limited by system size and low image quality. The TOMI scope removes these barriers with a handheld system, similar to an Otoscope. The clinical study clearly shows that TM has a statistically significant difference in its thickness between Normal (100 um), Acute (~180 um), and Chronic (300 um). The main barriers to commercialization may be the potential change physician practice to focus	8

biofilm (tympanic membrane) is displayed at roughly 70 frames per second on a screen [15].	on membrane thickness rather than the membrane itself. The system cost could be huge barrier to commercialization in the absence of reimbursement.	
Smartphone otoscope: This smartphone-based spectral imaging otoscope uses a multiplexed LED light source and series of lenses to capture images of the TM at different visible wavelengths from 405 nm – 700 nm. The system communicates with the smartphone for image capture, processing and display, but does not use the smartphone's light source [19].	Multispectral imaging in the visible range has been tried by many people including in [12]. An important improvement in this device is the miniaturization of optics and use of a smartphone, which decreases system size and, possibly, opens up non-clinical use scenarios. This device has potential to be used by parents as a screening tool, but the results do not instill confidence for diagnostics use. This is because the results do not show significant intensity differences between normal TM and the TM filled with liquid except for at 500 nm – 600 nm. The number of samples and the absence of statistical tests reduces the confidence of repeatability of the tests.	3
Smartphone Reflectometry: This smartphone-based device dubbed as "tricorder tympanometry" measures a TM's deflection properties at different frequencies to identify the presence of liquid in the middle ear. The phone's speaker plays 150 ms audio signals ranging from 1.8 to 4.4 kHz while a microphone detects both the incident	Although the technology can be used as an alternative to acoustic reflectometry, it cannot be used as a primary diagnostic device as this is not a recommended diagnostic standard. This device is a smart version of acoustic reflectometry where the tympanograms are analyzed with machine learning algorithm to produce results (normal ear, fluid filled bulging, fluid filled	3

wave from the speaker and reflected wave from the TM. In normal cases, the reflected signal will be resonated at multiple frequencies, resulting in a broadband spectrum with shallow depth. When the inner ear is filled with puss or fluid the TM's vibrational capacity decreases and the resulting output has less reflected energy, due to higher destructive interference. This results in much deeper reduction (deeper depth) of signal in resonated frequencies when compared to a normal TM [18].	retracted). As the authors point out, the device can be used as a screening tool to check the progression of the liquid presence, once it is confirmed by a doctor using an otoscope. Finally, as proposed by the authors the device has potential for use by parents and caregivers as a screening device in resource limited settings.	

The technologies presented in the table provide a curated list of middle ear imaging devices that has shown effective proof-of-concept in the past two decades. Although quite a few researchers have worked on improving the otoscope, only few technologies came close to commercialization. In fact, Photonicare TOMI scope [15] is the only device that has received FDA 510(k) clearance and SWIR otoscope is currently in the clinical trials. In summary, the ear imaging devices hit snag due to factors including not capturing the stakeholder (physicians) requirements, insufficient reimbursement, difficulties with device validation and regulatory clearance to name a few. Therefore, it is important to analyze all these devices to inform us on the existing gaps and design choices for a successful go-to-market device.

Based on our analysis and discussions with physicians, we came up with the following key design requirements to develop a device to diagnose middle ear effusion and commercialize successfully:

The proposed device should

1. Have the ability to see at least 2 mm on the lateral dimension of the tympanic membrane

2. Conform to existing standard procedures and leverage the existing, familiar otoscope model for device development
3. The device should be able to fit into both infant and adult ear. The device should work with <0.5 cm diameter of the speculum
4. Provide a quantitative and visual indication of presence and amount of the fluid behind the tympanic membrane
5. Cost should on the order of few hundred dollars, close to the price of video otoscope.
6. Produce images with sub 100 um feature resolution, and videos with atleast 10 Hz refresh rate for live imaging.

The following chapters provides discussion on the selected solution based on the above requirements and key results.

Chapter 3 | Vis-NIR Multispectral Imaging System

The availability of affordable sources and silicon-based detectors has increased the widespread use of NIR imaging for medical diagnosis. The widely used blood oxygen saturation (SPO2) measurement device exploit the relative absorption spectra of oxygenated and deoxygenated hemoglobin, with absorption 650 nm (red) and 900 nm (infrared) having greater affinity for deoxygenated and oxygenated hemoglobin respectively. Most of the tissues in the human body have an exponential increase in light transmission as the wavelength increases [22,23]. Therefore, low frequencies are used in various biomedical signal and imaging processing measurements as they can penetrate multiple tissues. Different blood components such as lipids, proteins, red blood cells (RBCs) and collagen absorb different wavelengths of light more prominently in the NIR and IR region than in the visible region.

Middle ear tissues have similar optical characteristics to the tissues investigated for other imaging applications. The diagnosis of middle ear fluid involves imaging the middle ear cavity through the translucent TM which is primarily made of collagen fibers and is largely transparent at higher wavelengths. The middle ear fluid can contain multiple components such as proteins, cells, blood, etc. A thin fluid is present behind the TM in case of OME, and a thick cloudy puss like fluid in case of Acute Otitis Media (AOM). Similar to the TM, middle ear fluids also transmit more light in higher wavelengths. Therefore, it is advantageous to use higher wavelength imaging for this application.

As discussed in Chapter 2, while there is prior art proposing multispectral imaging for ear imaging, most embodiments have been focused on the visible wavelength range (400-700nm), as is the case with traditional white light otoscopy. Schmilovitch et al. [16] proposed a spectrometric otoscope to image the middle ear, where they have used single-pixel measurement of reflection of tympanic membrane from 400 nm - 1000 nm. Although the initial results were encouraging, the unavailability of high-resolution image of the ear structures and the use of a spectrometer in a clinical environment can prove to be a problem.

Herein, we propose a multispectral imaging system to use two or more wavelengths in the Vis – NIR region between 600 nm - 1050 nm to image the middle ear structures. This

multispectral system exploits the attenuation properties of the TM, air, ossicles, and middle ear fluid at different, select wavelengths to produce images that has varying contrast difference between the areas that are filled with fluid and the areas that are filled with air and bone (ossicles). By subtracting these images, the presence, partial of full, or absence of middle ear fluid can be detected with high sensitivity.

3.1|Optical Properties of Middle Ear Tissues

The TM and middle ear fluid are the two major structures that contribute to light absorption and scattering in middle ear imaging. Therefore, it is important to consider the optical properties of these structures while selecting the wavelength range of interest for multispectral imaging. While discussing optical properties, we define the commonly used terms governing light interaction in our system, namely, scattering, reflection, transmission, absorption and attenuation. When photons impinge on a thin, translucent membrane, they are scattered. A portion of the photons that hit the membrane are reflected at the interface in multiple directions; this is known as diffuse reflection. The remaining portion of the light is transmitted through membrane in different directions; this is known as diffuse transmission. During transmission through a membrane or a medium (in this case, ear fluid), some of the light photons are absorbed, due to their affinity to particles present in the membrane. Attenuation is defined as the ratio of incident light intensity to detected light intensity and is not a material property. It is a function of diffuse reflection, transmission and absorption through the membrane and ear fluid.

Doladov et al. [21] studied the reflection properties of the TM from 400nm to 900nm on human cadavers. Carr et al. [8] performed e-vivo measurements of the TM's optical properties and those of various types of middle ear fluids over a much larger range (400nm -2000nm) and this served as background for this work.

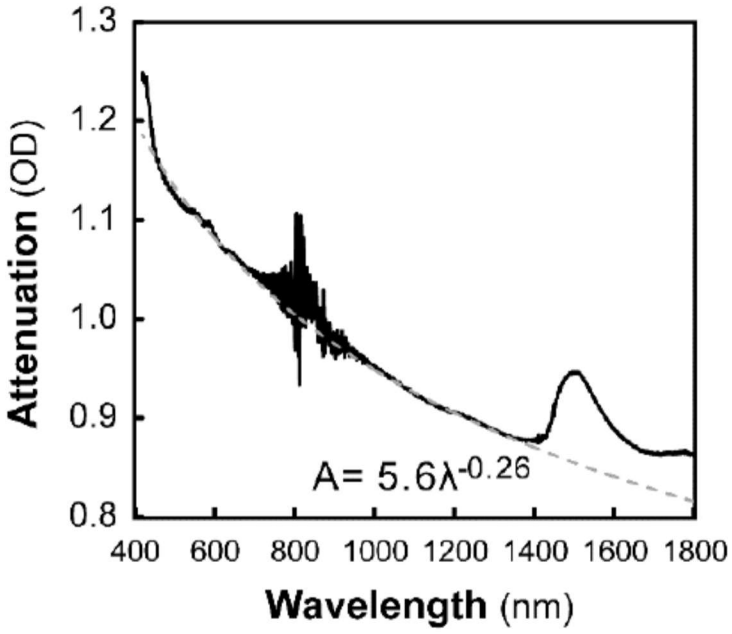

Figure 3.1 Attenuation properties of human TM samples extracted from pediatric patients, from [8]

The attenuation curve, reproduced in Figure 3.1, shows an exponential decrease in attenuation as wavelength increases, following an inverse power-law with a factor of -0.26. The attenuation properties of the TM follow those of other human tissues, which were measured earlier [22,23]. nIR wavelengths show very low attenuation in tympanic membrane which means more light can be transmitted through and provides an opportunity to look at the components (fluid) behind the translucent membrane. It is important to note that while attenuation will decrease significantly moving into SWIR and the IR region, but specialized optics and photon detectors are needed to capture the image, which would drive up the cost of the device significantly. Therefore, we have focused on nIR wavelengths up to 1050 nm, which still provide much lower attenuation than the visible wavelengths. The attenuation curve in Figure 3.1 shows high noise around 800-900nm that is caused by inefficiency of the grating that was used in this experiment [8]. Therefore, we do not expect this to be an issue as we are not using any grating in the system and it is expected that the membrane will follow the power curve in ideal scenario.

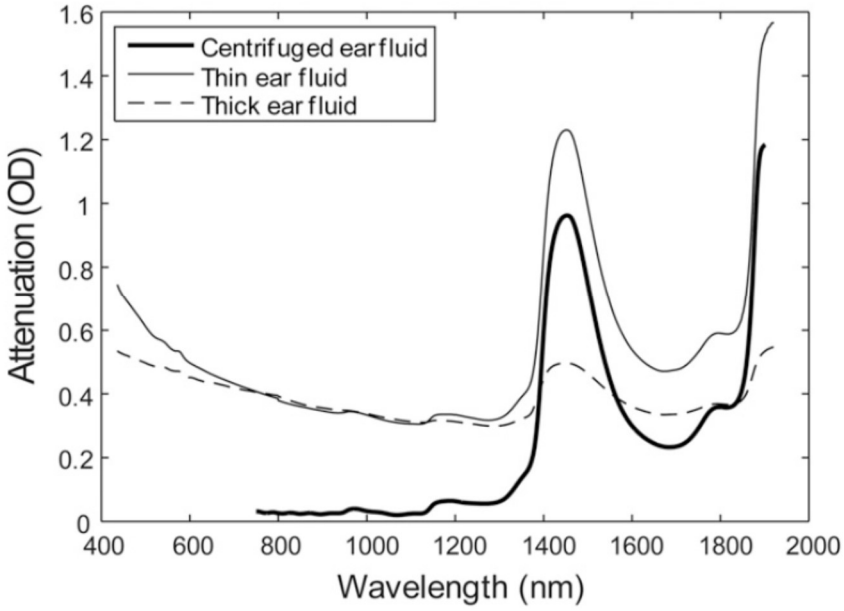

Figure 3.2 Attenuation of thin serous, mucous serous fluid, and centrifuged ear fluid, from [8]

The attenuation curve, reproduced in Figure 3.2, for middle ear fluid also shows a decrease in attenuation with increasing wavelength. The curve appears to plateau as it reaches NIR wavelengths and the attenuation follows an inverse power response similar to that TM in the region of our interest (visible – NIR). The attenuation properties of the ear fluid show very high attenuation around 1400 nm, but otherwise the attenuation remains relatively constant. Here it is important to note the relative optical properties of thick and thin ear fluid, indicators have not been studied extensively. A difference in attenuation between the two types of fluid at SWIR (~1400 nm) wavelength could mean that the SWIR [8] device might be able to differentiate between AOM and OME. But, the primary objective of our multispectral imaging system is to detect the fluid with high sensitivity and, therefore, similar attenuation response for both thin and thick ear fluids in VIS – nIR does not affect the functional properties of the proposed device.

With the goal of imaging both the TM and detecting the presence of fluid behind it, it is important to strike a balance between attenuation of tympanic membrane and that of ear fluid at different wavelengths. High relative attenuation by TM would flood the image with reflected light while low relative attenuation would result in only middle ear structures being visualized and not the and not the membrane. In an ideal scenario, we would need a wavelength which has overall low attenuation for the TM, so that it produces just enough reflection to image the

membrane, and much higher attenuation for ear fluid. This way the photons that are transmitted through to the fluid are absorbed due to wavelength specific affinity and only a tiny fraction of the photons are reflected back to the detector. This would produce a high contrast between the fluid which is a high absorption, low reflection medium and a reference, such as the ossicles, which have very high reflection and negligible absorption and this contrast difference varies as a function of wavelength. Thus, by subtracting images with different contrast levels taken at multiple select wavelengths, the middle ear area that is filled with fluid can be highlighted to allow physicians to distinguish ear fluid from the rest of structures in the image. To achieve high contrast between ossicles and ear fluid, and to image the tympanic membrane, we have selected 600 nm to 1050 nm wavelength for this multispectral imaging approach. This work presents a starting point for the development of low cost, high performance "Vis-NIR" multispectral otoscope. We concentrated on evaluating the multispectral concept in phantoms that mimic the properties of the ear tissue to show the proof-of-concept.

3.2|Phantoms as test materials

Because this is early stage work, a suitable tissue phantom for the TM, middle ear structure, and middle ear fluid that was identified in the work of Carr et al. [8] was used in this experiment. This is shown in Figure 3.3 and consists of multiple parts: (a) represents the middle ear shapes and angles and is 3D printed using PLA plastic filament. (b) represents the TM and consists of a thin disc of platinum silicone (Dragon Skin™ FX- Pro™) that was first cast in a sheet and then cut into 20mm discs. The TM is then assembled on top of the 3D printed structure to create the complete middle ear structure as shown in Figure 3.3 (c) and (d). A small hole in the rear of the phantom is used to fill the inside with liquid.

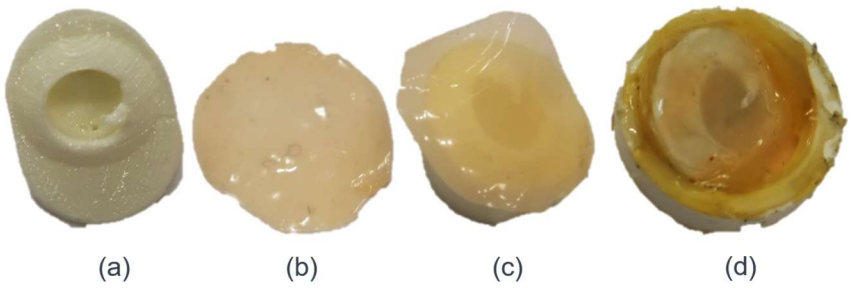

Figure 3.3 Middle ear and tympanic membrane phantoms in the order of its assembly

It was important to measure the optical properties of the TM component (b) before experimentation. A Fianium Supercontinuum laser and acoustic optical tunable filters were used to generate coherent light ranging from 600nm-1050nm. The TM component (b) was sandwiched between the light source and an Ocean Optics spectrometer (detector) to measure the light intensity after travelling through the membrane then it was removed to measure the reference or 100% transmission. The ratio of incident light (100% transmission) intensity to intensity after traveling through the membrane is used to measure the attenuation properties of the membrane, as shown in Figure 3.4. The attenuation follows the inverse power law trend with increase in wavelength, which is similar in shape to the human TM membrane response in Figure 3.1. The changes in absolute values of attenuation in phantom model could be due to its increased thickness and the absence of biological components when compared to the human TM. While the human TM can measure 100-350 um in thickness under normal to diseased conditions, the phantom TM is made to be 500 um thick, so as to have better stability while testing. We believe this will not have a significant impact on our results as the membrane stretched during the assembly and the final thickness could be close to that of the human membrane.

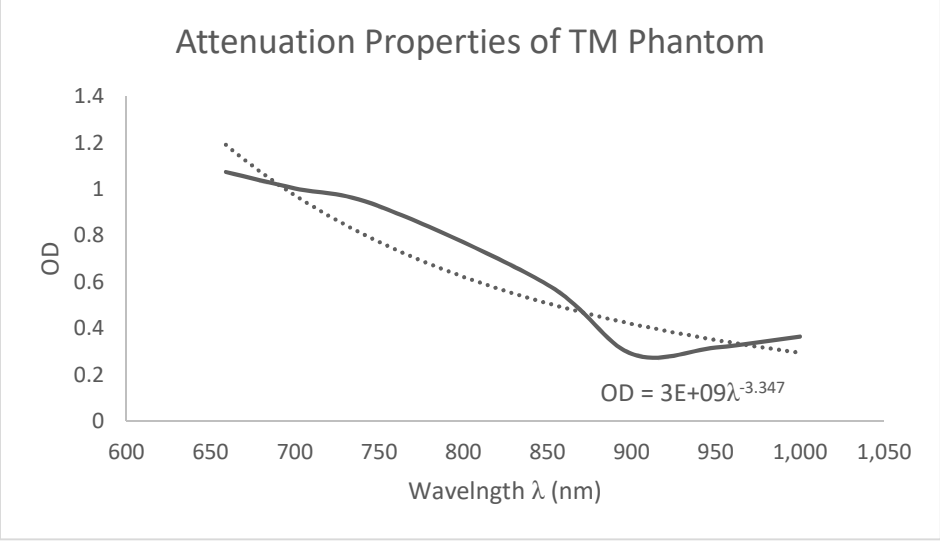

Figure 3.4 Attenuation properties of TM phantom made using a platinum silicone mold

As mentioned in the introduction of this chapter, middle ear fluid can be a thin serous fluid in the case of Otitis Media with Effusion (OME) or thick mucus (puss-like) fluid in case of Acute Otitis Media (AOM). As shown in Figure 3.2, the two different fluids do not have a

significant difference in attenuation properties in the wavelength(s) of interest. This suggests that in our selected range of wavelengths a single fluid can be used to mimic both conditions. Carr et al. [8] identified unconcentrated orange juice as a substitute middle ear fluid for the proof-of-concept purposes. Later work could focus on differentiating different fluids types.

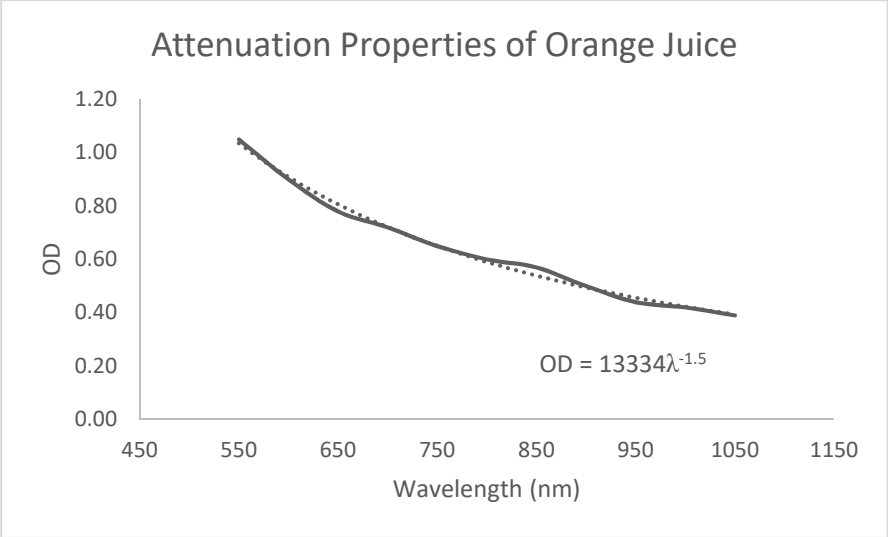

Figure 3.5 Attenuation properties of orange juice as reported in Carr et al. [8]

Figure 3.5 shows that the attenuation curve follows inverse power law where attenuation decreases with a factor -1.5 with every unit of increase in wavelength. Although, we do not have the attenuation equation for the ear fluid, one can compare the Figure 3.5 and Figure 3.2 and find that both follow the same trend. We can also find that there is some deviation between the absolute attenuation values of middle ear fluid and orange juice, but this is expected since it is difficult for phantoms to replicate exact same properties. Since we are only interested in the change in attenuation between visible and NIR wavelengths, orange juice is a sufficient phantom for proof-of-concept testing. Moreover, we are not seeking to measure specific optical properties, rather detect relative differences, which is expected to be more robust.

3.3|Modeling the light scattering in phantoms

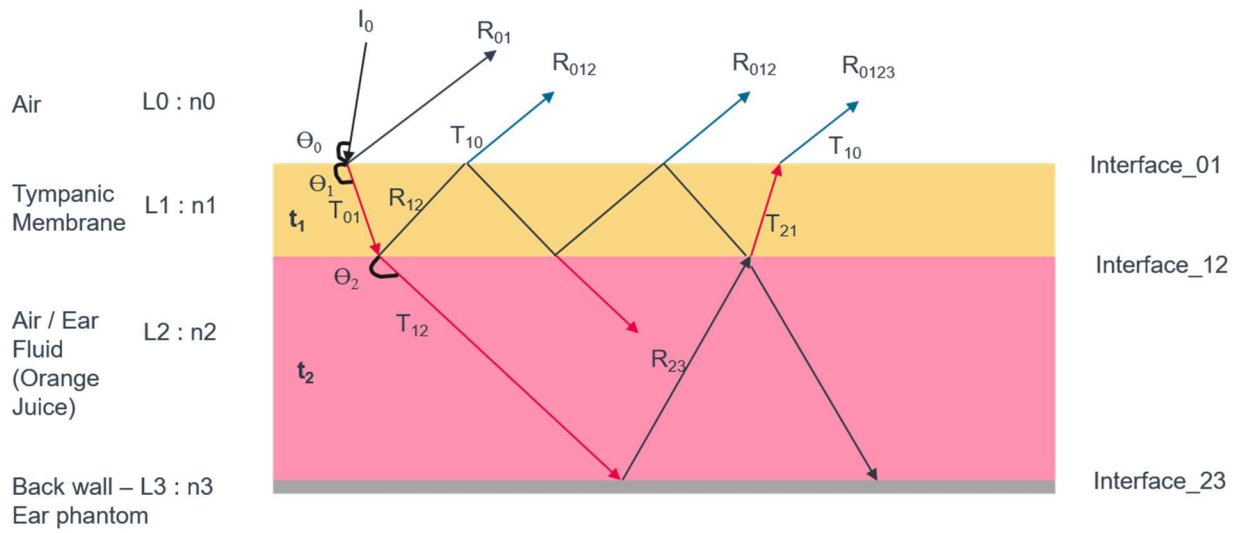

Figure 3.6 Light scattering model of the ear phantom using phase-based transmission and reflection

Based on the known optical properties of the phantom and light source, we modeled the ear phantom as a staggered layer, where light scattering transmission or reflection occurs due to phase changes (change in refractive index) at the interfaces. A generic model for reflection of light in thick non-diffusing layers has been demonstrated in multiple works [24,25]. The model implemented in this work used the extension of William Klepper's model for stacked layers with different refractive indices developed by Simonot et al. [25].

Shown in Figure 3.6, the model consists of four layers: The top layer (L0) consists of air with a refractive index of n0, a second layer (L1) represents the TM with a refractive index of n1, the third layer (L2) is middle ear fluid/air with a refractive index of n2, and the model ends with back wall layer (L3) made up of 3D printed PLA plastic with a refractive index of n3. The TM and fluid layer thickness are many times higher than the wavelength. Therefore, the chances of Rayleigh or Mie scattering in these conditions are almost nil and not considered in the model. In our model, we consider three interfaces as there are n-1 interfaces and n layers. Interface_01 is the interface between Air (Layer 0) and TM (Layer 1), Interface_12 is the interface between TM (Layer 1) and Ear Fluid (Layer 2), and Interface_23 is the interface between Ear Fluid (Layer 2) and Back wall layer (Layer 3).

Due to the nature of the middle ear structure, the final image / output produced is function of reflected light photons from the sandwiched structure as shown in the figure above. In this experiment, the source is a supercontinuum laser, therefore the incident light and the reflected light are assumed to be coherent with no intrinsic polarization. The polarization properties of the light are not expected to change even the source is shifted from Laser to LEDs. Therefore, horizontally and vertically polarized photons are assumed to be present in an equal amount as in the case of natural light and the incident power for such lights can be calculated with Eq. 1.

$$\text{Incident radiant power, } w_i = \frac{1}{2}\left[w_i^{(p)} + w_i^{(s)}\right] \text{ ---------- (1)}$$

A generic equation for reflection between two layers (j, k) with different refractive indices (Θ_j, Θ_k) for p-polarized and s-polarized light can be formulated as follows:

$$R_{jk}^{(p)}(\theta_j) = \frac{tan^2(\theta_j - \theta_k)}{tan^2(\theta_j + \theta_k)} \quad \text{---------- (2)}$$

$$R_{jk}^{(s)}(\theta_j) = \frac{sin^2(\theta_j - \theta_k)}{sin^2(\theta_j + \theta_k)} \quad \text{---------- (3)}$$

Since the final irradiance contains an equal amount of p and s polarized light photons, the reflection signal contains an equal amount of

$$R_{jk}(\theta_j) = \frac{1}{2}\left[R_{jk}^{(p)}(\theta_j) + R_{jk}^{(s)}(\theta_j)\right] \quad \text{---------- (4)}$$

The scattering involves only transmission and reflection at each interface, therefore the transmission equation can be written as follows. The same property applies to both polarizations.

$$T_{jk}(\theta_j) = 1 - R_{jk}(\theta_j) \quad \text{---------- (5)}$$

In the model, we assume that the incident angle of light (Θ_j) on a specific layer is known and from Snell's Law of Refraction

$$n_j \sin\theta_j = n_k \sin\theta_k \text{ --------- (6)}$$

we can determine the resulting angle of refraction, Θ_k.

$$\theta_k = sin^{-1}\left[\frac{n_j}{n_k}.\sin\theta_j\right] \text{ ---------- (7)}$$

Due to the nature of the light, reflection and transmission are assumed to have commutative properties. So, the reflection at interface j - k and vice versa can be written as follows.

$$R_{jk}(\theta_j) = R_{kj}(\theta_k) \quad \text{---------- (8)}$$

The final irradiance, returning from the TM to the detector, is the sum of all reflected irradiances from each of the interfaces. Since we have three interfaces, we start by calculating the irradiance at each layer w_{rk}. Here k denotes the interface number. Irradiance at Air / TM interface can be written as follows,

$$w_{r0} = w_i . R_{01}(\theta_0) \quad \text{---------- (9)}$$

The irradiance due to the reflection and transmission from the TM and orange fluid interface is due to transmission from layer 0 to 1 (T_{01}), reflection at the interface_12 (R_{12}), and the transmission through the layer 1 (t_1), and the final transmission from layer 1 to 0 (T_{10}). The irradiance equation can be written as follows,

$$w_{r1} = T_{01}(\theta_0) . t_1^2(\theta_1) . R_{12}(\theta_1) . T_{10}(\theta_1) . w_i \text{ -------- (10)}$$

Transmission t_1, through the TM happens twice as shown in Figure 3.6. During the transmission, a portion of the light is attenuated due to the absorption and, therefore, the amount of light transmitted thorough the TM can be written using the Beer-Lambert law as follows,

$$t_1 = e^{\frac{\propto_1 d_1}{\cos\theta_1}} \quad \text{---------- (11)}$$

where d_1 is the thickness of the TM, $\propto_1$ is the absorption coefficient which can be derived from TM attenuation curves, presented earlier in this chapter. A similar equation can be written for transmission through ear fluid/orange juice.

The equation 10 considers only reflection and transmission from single rays. Upon closer look at the Figure 3.6, we can find that for every light ray that enters the layer 1, There can be 'n' internal reflection at interface_12 (shown by black lines), and 'n-1' reflection and transmission at the interface_01 (as signified by two R_{012} light rays) . As mentioned in Simonot et al. [25], the generic equation that includes multiple internal reflections and transmissions can be written as follows,

$$w_{rn} = T_{01}(\theta_0) . [R_{10}(\theta_1)]^{n-1} . [R_{12}(\theta_1)]^n . t_1^{2n}(\theta_1) . T_{10}(\theta_1) . w_i . \text{ ---------- (12)}$$

The total reflected irradiance w_r, is a sum of all the reflected irradiances w_{rn},

$$w_r = w_i.R_{01}(\theta_0) + \frac{[T_{10}(\theta_1)]^2.[R_{12}(\theta_1)]^1 \cdot t_1^2(\theta_1)}{1-[R_{10}(\theta_1)]^1.[R_{12}(\theta_1)]^1 \cdot t_1^2(\theta_1)} . w_i$$ ---------- (13)

The ratio of reflected irradiance, w_r to incident irradiance, w_i gives the total reflected light through interface_01 and interface_12, R_{012}.

$$R_{012}(\theta_0) = R_{01}(\theta_0) + \frac{[T_{10}(\theta_1)]^2.[R_{12}(\theta_1)]^1 \cdot t_1^2(\theta_1)}{1-[R_{10}(\theta_1)]^1.[R_{12}(\theta_1)]^1 \cdot t_1^2(\theta_1)}$$ ---------- (14)

The above equation is the same for the p-polarized and s-polarized light. Rewriting equation (4) gives us,

$$R_{012}(\theta_0) = \frac{1}{2}\left[R_{012}^{(p)}(\theta_0) + R_{012}^{(s)}(\theta_0)\right]$$ ---------- (15)

Since the transmission equation can be rewritten as reflection using equation 5, the transmission equation is not presented here. Our final result is the total reflection of light through all the interfaces R_{0123}. Equation 14 can be easily extended to include reflection through the ear fluid layer (L3) by referring to Figure 3.6.

$$R_{0123}(\theta_0) = R_{012}(\theta_0) + \frac{[T_{210}(\theta_2)]^2.[R_{23}(\theta_2)]^1 \cdot t_2^2(\theta_2)}{1-[R_{210}(\theta_2)]^1.[R_{23}(\theta_2)]^1 \cdot t_2^2(\theta_2)}$$ ---------- (16)

Equation 16 presents the analytical model for the reflected light received by the detector, based on a simple phase-based transmission and reflection model from the multilayered set-up (phantom). This model does not take in to account diffuse reflection that arises from the TM. Since a coherent laser light source is used, the system can produce interference at the surface of the TM. In addition, the model may also be limited by unaccounted for wavelength dependency of refractive indices, but such information was difficult to obtain for our phantom materials. Adding these parameters will improve the models, but is not essential, as the objective is to observe the output trends resulting from the attenuation changes in the TM, and ear fluid at different wavelengths.

The model was implemented in MATLAB with the following parameters: Membrane thickness of 300 um, Ear fluid thickness of 1 mm, and with the absorption coefficients retrieved from Figure 3.4 and Figure 3.5. The refractive indices of all the materials used in the experiment were obtained from material property data. The average refractive index of the orange juice (n_{OJ}) is 1.3532 to 1.36 [27] which is very close to refractive index of blood (n_{blood}), 1.36 [26]. For the TM, made of platinum silicone, we used the refractive index of liquid silicone n_{TM} = 1.40 [28]. The back wall is made of PLA plastic with a refractive index of 1.46 [35].

The model was run for a sweep of wavelengths from 450 nm to 1100 nm for both a fluid and an air filled middle ear and the results are shown in Figure 3.7 below.

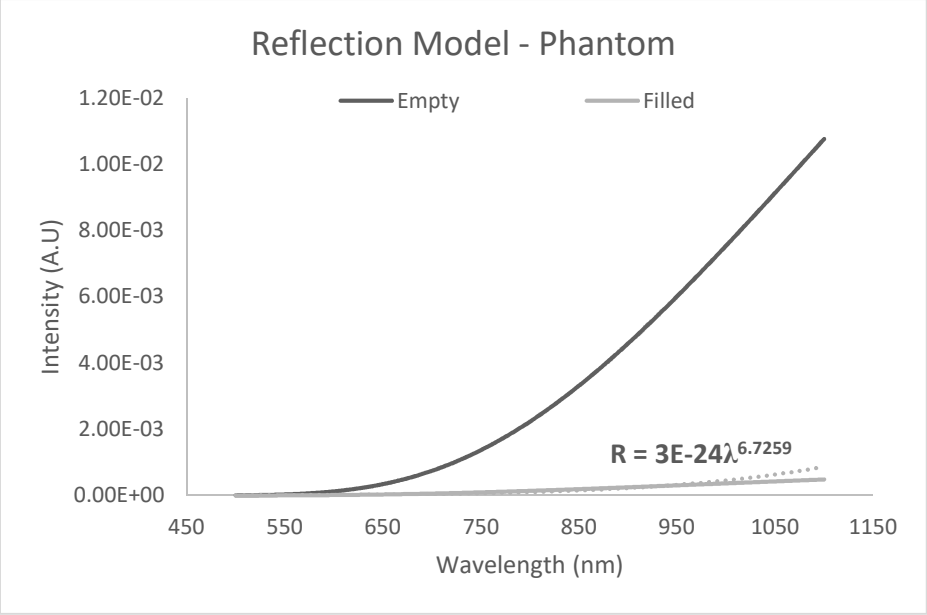

Figure 3.7 Results from light scattering model of the phantom

The figure shows that when the phantom is filled with fluid, the light intensity from the ear phantom doesn't change considerably in the visible and early NIR wavelengths (500-850 nm), while a significant change is evident in wavelengths of 850 nm and beyond. This was later validated experimentally. As shown in the Figure 3.7 above, both the filled and empty case follows a power law curve, but the empty case has greater intensity across all wavelengths. This is due the fact that both TM and middle ear fluid follows an inverse power law curve for light attenuation as shown in Figure 3.4 and Figure 3.5. The empty case has much higher intensity since the air does not provide any attenuation whereas the orange fluid filled phantom has different attenuation at different wavelengths. These model results furthered our hypothesis that a multispectral imaging system from Vis - NIR could enable detection of a full or partially filled middle ear. For this modelling exercise, the incident powers at each wavelength were the same, however, for this method to work the input powers must be calibrated so that the reflected intensities are equalized for empty phantoms across the wavelengths of interest, i.e. the system response is relatively flat. Therefore, once the phantom is filled, the output signal will be dominated by the attenuation provided by the fluid.

A detailed calibration procedure is discussed in next chapter. A detailed study of how the model parameters such as incident angle, membrane thickness and fluid thickness (depth level of the fluid present) affect the final reflected signal are also presented in the next chapter.

3.4|Experimental set-up

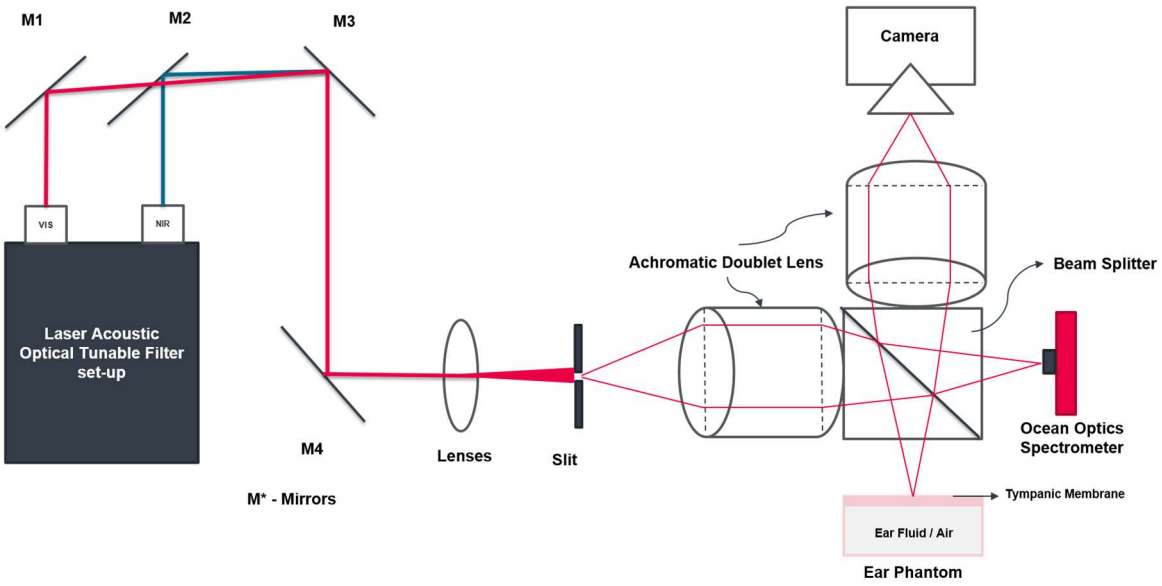

Figure 3.8 Multispectral Imaging System Schematic

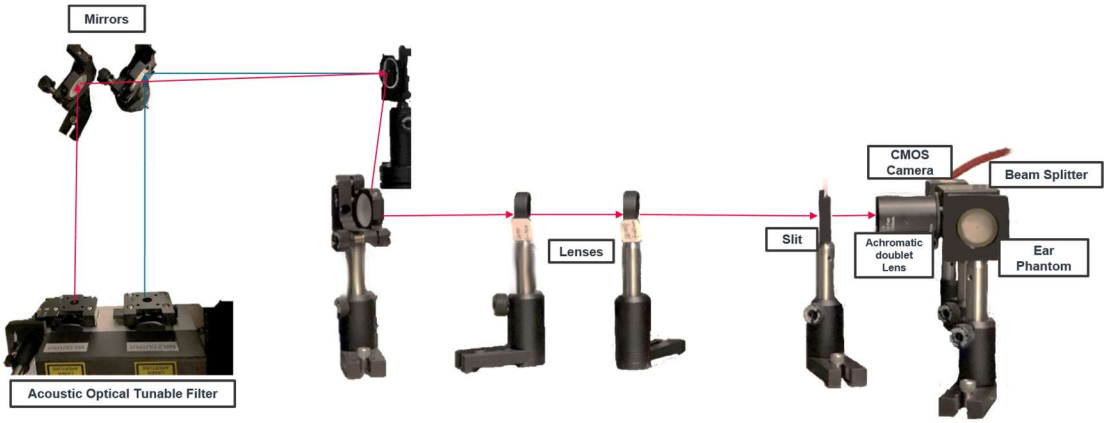

Figure 3.9 Actual set-up of the Multispectral Imaging system

In parallel with the modelling work, a benchtop multispectral optical imaging system was built. Figure 3.8 and Figure 3.9 show the schematic and the real set-up of the optical imaging system. A supercontinuum laser, (SuperK Compact^{TM}, NKT Photonics) was used as a light source, and a dual-channel (VIS-NIR) Acoustic Tunable Optical Filter (SuperK Select^{TM} Multiline Tunable

Filter) was used to deliver the wavelengths of interest. A series of mirrors and lenses directed the light to the targeted location. An adjustable slit of 2 mm diameter and an Achromatic Doublet Lens (MAP103075-B, Thorlabs), which has an anti-reflective coating in 650nm-1050nm to avoid stray light and non-specific wavelengths, was used to select the narrow band of wavelength and focus the light respectively. The imaging system was set-up in an "epi-configuration", whereby the source and imaging plane of interest are orthogonal to each other and the detector (camera) is coaxial with the image plane to allow for the reflected light to be captured. A UV-NIR Beam splitter (BSW26, Thorlabs) was used to divide the light 50/50 between the phantom target and a spectrometer (USB 3000+, Ocean Optics). The resulting image was captured by a 1280x1024 pixel monochrome CMOS camera (DCC3240N), which has relatively good sensitivity in the NIR region compared to normal CMOS cameras. The spectrometer was used to confirm the spectral characteristics of the light at each wavelength, including power and bandwidth, as shown in Figure 3.10. The spectrometer did not analyze the returned image and would not be present in a final system.

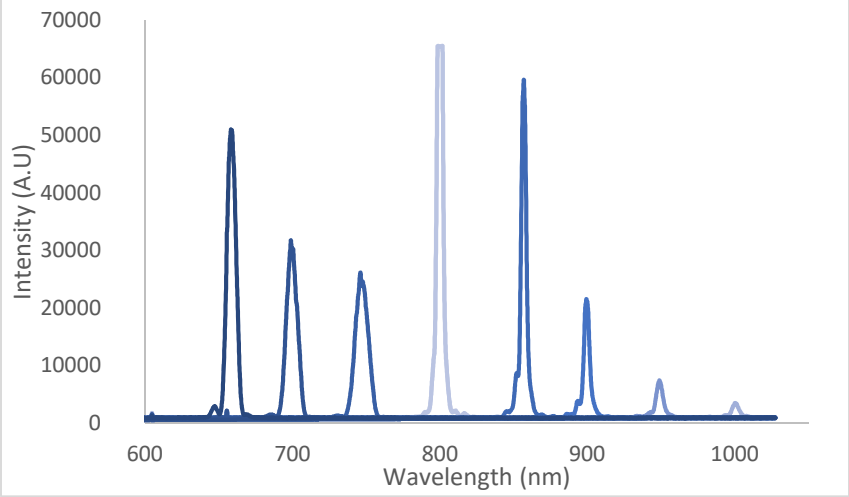

Figure 3.10 Relative Intensity measurements from the Spectrometer

The experimental results and spectral conditions are provided in Figure 3.10 and Figure 3.11. The results show the middle ear phantom partially filled with orange juice and imaged under wavelengths from 650 nm to 1000 nm. It can be seen that the intensity differences a.k.a contrast between the liquid areas (red) and the background (blue) is low in the visible light region. As we

approach 900 nm, there seems to be a slight increase in contrast, but the liquid is even better differentiated at 1000 nm. The multispectral imaging system exploits this contrast difference between visible and NIR wavelengths to detect and highlight the fluid. The intensity of the empty region is expected to be constant across wavelengths and is not considered for contrast measurement as the empty area can change between experiments and empty areas close to fluid areas can have intensity variation between wavelengths A detailed analysis of the system sensitivity using image contrast difference and an image processing algorithm to enable detection of the liquid qualitatively is discussed in the following chapter.

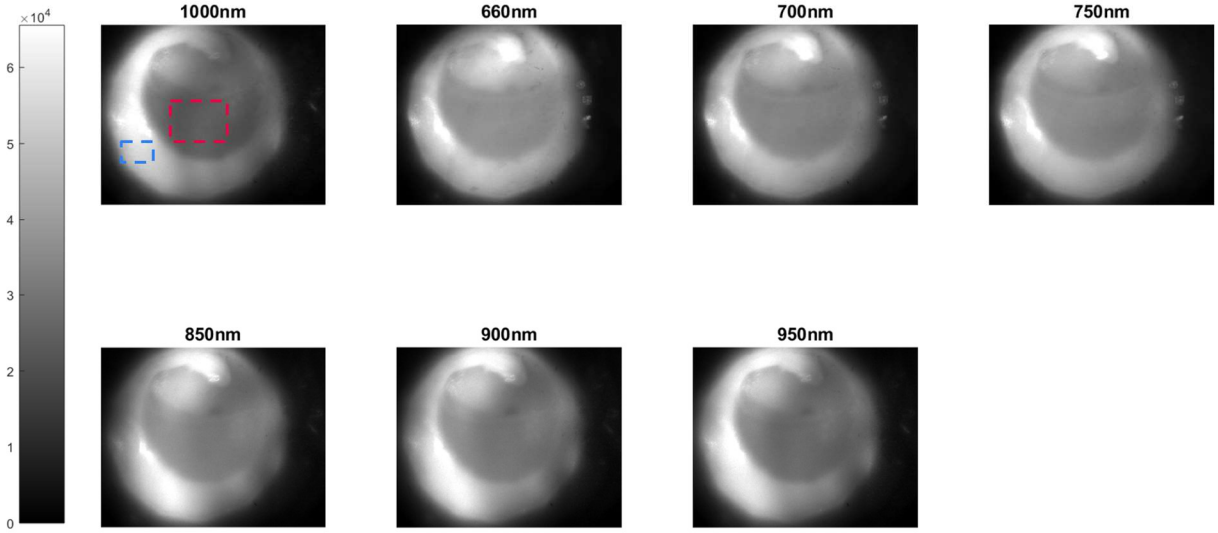

Figure 3.11 Experimental results with orange juice filled up to 70% inside the phantom

We performed further experiments with fluids with different refractive indices, fluids filled to various levels inside the phantom, and with the phantom angled with respect to the incident light. The purpose was to obtain robust proof-of-concept results and understand the limitations of the system and Table 3.1 provides a summary of our experimental design. The following chapter discusses the results in detail.

Table 3.1 Experiment design matrix

Experiment Condition	Images acquired from 650 -1000nm with 50nm increments Each trial began with calibration with a standard white surface to equalize reflection across wavelengths.
Orange Juice (Refractive Index, n = 1.36)	The liquid is filled to various levels inside the phantom (Empty, 20%, 50%, 70% filled) and images are acquired at the above wavelengths. Two repeats of this condition are performed.
Refractive Index Standard (n = 1.33)	The liquid is filled to 70% inside the phantom and images are acquired at the above wavelengths.
Refractive Index Standard (n = 1.33) diluted with 50% Orange Juice	The liquid is filled to 70% inside the phantom and images are acquired at the above wavelengths.
Refractive Index Standard (n = 1.46)	The liquid is filled to 70% inside the phantom and images are acquired at the above wavelengths.

Chapter 4 | Results and Discussion

This chapter discusses the calibration procedure for the multispectral experimental set-up, presents results from the ear phantom imaged at different wavelengths and using different light sources (laser and LED) and comments on the methods effectiveness at detecting the presence or absence of fluid. We also discuss the results of the analytical model described in Section 3.3, and compare them to our experimental data to define system parameters.

4.1|System Calibration

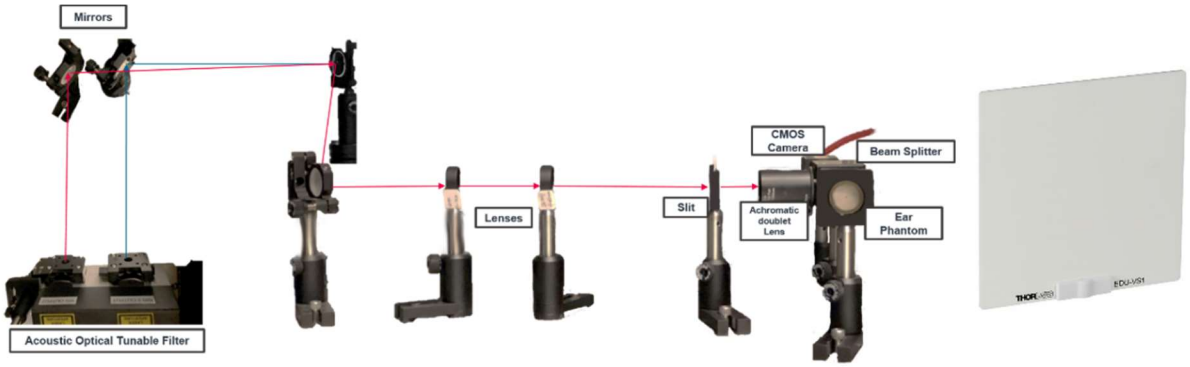

Figure 4.1 Multispectral imaging set-up with a calibration standard

As discussed in the experimental set-up Section 3.4, the experimental system used a supercontinuum laser to generate different wavelengths of light in Vis – NIR region. Each wavelength has different source power, as shown by the intensity graph in Figure 3.10, and the CMOS camera has also different quantum efficiency across all the wavelengths. These variations would overshadow the ability to observe different contrast and negate the advantage of wavelength specific light attenuation of TM and Ear fluid. Therefore, the goal of calibration is to equalize the source, and detector variations and produce images of empty phantoms that have equal intensity across all wavelengths. To accomplish this, a white polystyrene screen (EDU-VS1, Thorlabs), shown in Figure 4.1, which has a smooth finish on one side and matte finish on the other, is placed at the same position as the ear phantom, with smooth finish facing the incident light. This gives a uniform, diffuse reflection that is similar to TM and also enables observation of interference patterns generated by the coherent laser source. Using the screen and the camera,

a series of images were acquired from 660 nm to 1000 nm at an interval of 50 nm. The reflected intensity was measured and the laser power was modified till equal intensities are observed across all wavelengths. Figure 4.2 shows the results where interference patterns are more visible in NIR wavelengths, as compared to the visible wavelengths, which has the potential to interfere with qualitative visual analysis. Figure 4.3 provides mean intensity for each wavelength, where it can be seen that the intensities now are equalized across the spectrum.

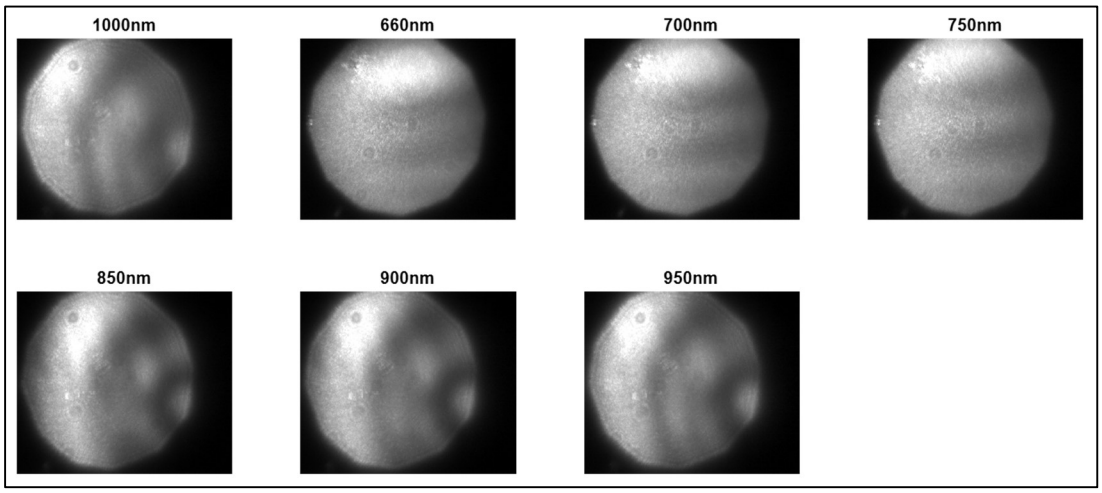

Figure 4.2 Intensity equalized images from standard reflectance surfaces.

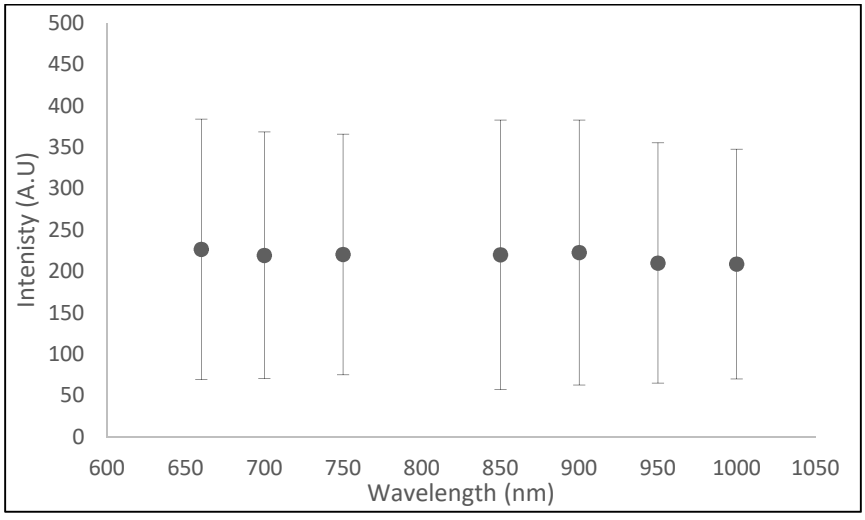

Figure 4.3 Mean intensity and standard deviation plots from the standard calibration surface.

Even though the intensities are equalized across the Vis – NIR spectrum, the intensity variation as shown by standard deviation is high. This is due to the interference pattern created by the coherent light source and this can affect the sensitivity of the system by 20 - 30%.

Therefore, when comparing between two images taken at different wavelengths, assuming the minimum intensity to be less than 100 A.U, and maximum intensity be close to 1000 A.U, the intensity deviation shown in the figure above could contribute to a contrast change of 0.2 or higher. Thus, the difference in contrast should be greater than this value in order to differentiate the liquid from the ossicles and areas of tympanic membrane that are not filled with liquid. Since the empty phantom is also a diffuse reflective surface, this calibration will help to produce images with uniform intensity and variation that is similar to or lower than that with calibration standard.

4.2|Detecting fluid contrast

The primary objective of our device is to detect the presence of fluid in the middle ear with high sensitivity. We experimented with varying fluid levels and selected near filled (~70%) conditions within the phantom to analyze the sensitivity of the set-up and investigate the quantitative difference between different wavelengths. Contrast is a good measure of the difference in pixel intensities between regions in the image. The multispectral imaging method relies on the contrast between areas of the middle ear such as ossicles and fluid and the difference in contrast between wavelengths. We measured and compared Weber contrast across all the wavelengths of interest for the empty and filled conditions. Weber contrast is defined as,

$$C_w = \frac{I_{max} - I_{min}}{I_{min}}$$

The I_{max} and I_{min} values are highlighted in red and blue, respectively, in both empty and filled images in Figure 4.4 at 660 nm and 1000 nm. The empty and filled images were captured from 650 nm to 1000 nm at intervals of 50 nm and only one representative image for empty and full is shown for visible and NIR wavelengths respectively.

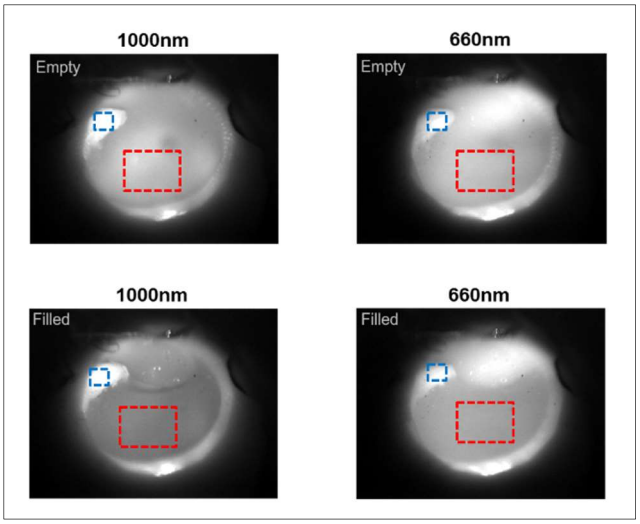

Figure 4.4 Empty phantom (top) and orange juice filled (bottom) ear phantom with the ossicles marked in blue and the fluid -filled region in red.

It is difficult to see a visual difference between empty and filled images when illuminated with 660 nm, which shows that it would be difficult for doctors to detect fluid with a visible light-based otoscope alone. In case of NIR, the 1000 nm image shows an improvement in contrast between the empty and filled phantom, however it is still open to subjective interpretation. In the experimental scenario, the presence of fluid was known a priori, however, in the real world there will not be an empty ear drum to serve as a baseline for comparison. Therefore, we sought a baseline area of the image, where the reflectance does not change with wavelength. In the ear the ossicles, marked in blue, serve this purpose. For this contrast analysis, we measure and compare intensities in the fluid filled tympanic membrane against this reference region. This is done to demonstrate viability of the proposed method where two or more images, taken at different wavelengths, can be compared to each other to visually highlight the fluid filled area in a way that is not possible with traditional otoscope. The developed technology, does not rely on comparison against the blue-marked region.

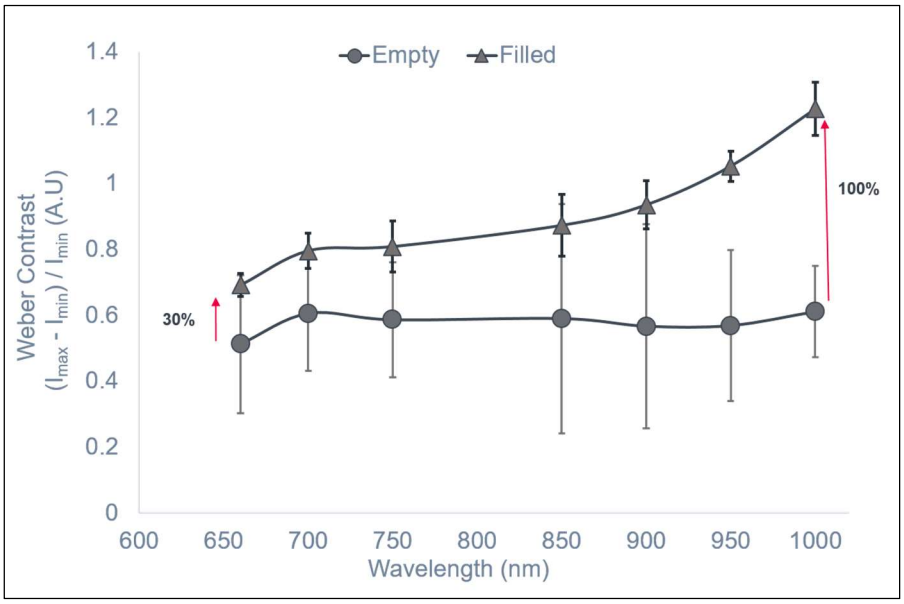

Figure 4.5 Weber Contrast comparison between Empty and Orange juice filled phantom as shown in Figure 4.4

Figure 4.5 shows key results from our experiments. Weber contrast is measured by measuring intensities in reference (ossicles) and areas that are empty or filled with fluid as shown in Figure 4.4. First, the calibration procedure described in Section 4.1 was followed, then images were taken for each wavelength. The scatter plot shows the Weber contrast difference between empty and filled phantoms across the visible and NIR region. The empty phantom shows almost flat contrast across the entire Vis – NIR region. Between empty and filled there is a marginal increase in contrast from 660 nm to 850 nm, 30-40%, but a significant change in contrast starts after 850 nm, approximately 80-100%. This contrast difference agrees with the results predicted by our reflectance model and referenced in Figure 4.7 Reflectance Model output using fluids with different refractive indices. However, one should note that the intensity variation in the empty phantom are on par with those due to interference effects, shown in Figure 4.2. The intensity variation is reduced in the filled phantoms as attenuation due to light absorption in fluid filled areas contribute heavily to the output as opposed to surface reflection in case of empty phantoms.

It is important to compare the performance of our system with similar results in the literature, particularly the work of Carr et. al [8]. Carr reported a 4x increase in contrast between an empty and filled phantom using SWIR imaging at 1300nm, compared to only a 2x increase in

the visible wavelength. Comparatively, our system reported 1.3x increase in visible and a 2x increase in NIR wavelength. Although, a high difference between empty and filled contrast values are important in order to distinguish fluid in single spectral systems, such as a visible otoscope and the SWIR, a multispectral system needs to compare the contrast at two different spectrums to detect the presence or absence of the liquid. A negligible contrast difference between the visible (660 nm) and NIR (1000 nm) points to the absence of fluid behind the membrane, whereas an 80% or more increase in contrast could point to the presence of fluid. Therefore, a contrast comparison or image subtraction between different wavelengths has the potential to better the fluid detection capacity of the visible otoscope and equal the fluid detection capability of the SWIR system at a fraction of the cost. The fluid detection algorithm is further discussed in the image processing section.

4.3|Testing system sensitivity using fluids with different refractive indices

Now, it is important to understand the limitations of our system and optimize the design parameters for further development. Even though the refractive index of the orange juice matches closely with that of blood, the actual refractive index of the ear fluid varies slightly between the thin serous fluid in the case of OME and thick mucous fluid in case of AOM. Therefore, we experimented filling the phantom with refractive index fluids as follows:

1. Refractive index standard - n1.33
2. Refractive index standard - n1.33 mixed with 50% orange juice (~n1.345)
3. Orange juice (Refractive index ~ 1.353 – 1.36)
4. Refractive index standard 1.46. Although this index is unlikely, we tested with this fluid to compare the results and increase the robustness of our theoretical model.

Attenuation difference in fluid between different wavelengths is not just due to the refractive index change, but also due to the absorption coefficient of the fluid. This is investigated by testing with both orange juice and a refractive index standard fluids which have flat absorptions coefficients across wavelengths.

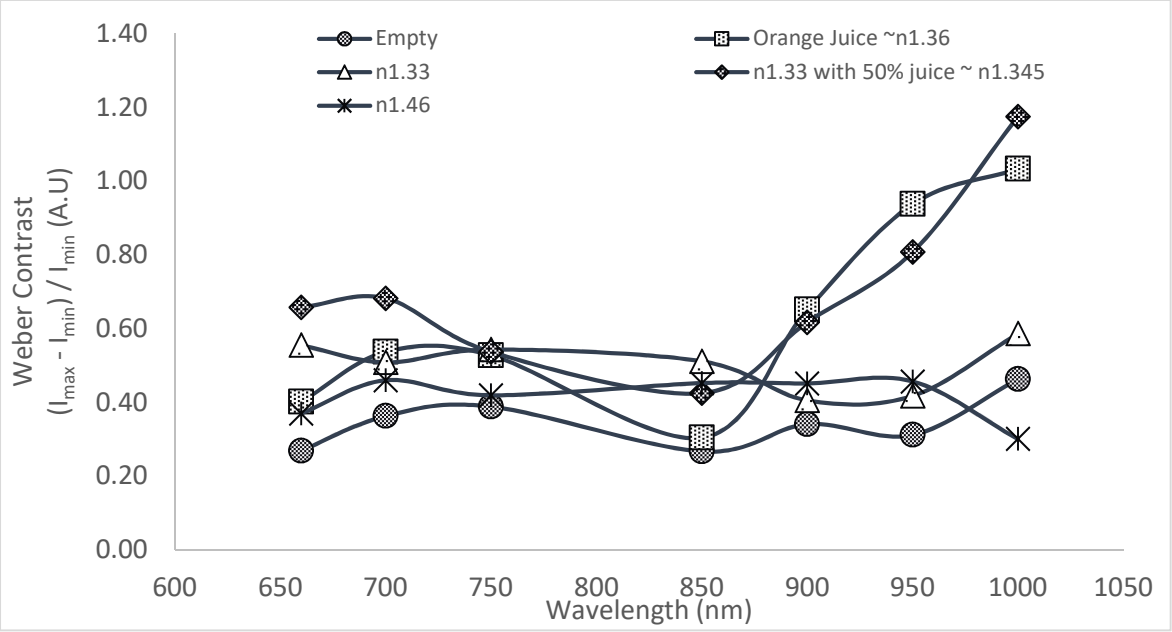

Figure 4.6 Weber Contrast comparison between fluids with different refractive indices

The graph in Figure 4.6 shows the Weber contrast, for both an empty phantom and one filled with orange juice and the various refractive index fluids. As expected, contrast remained flat throughout the entire range (650 nm to 1050 nm) for the empty and n1.33 and 1.46 standard fluid cases, while it increased with increasing wavelengths for pure orange juice and the 50% mix with n1.33. The contrast difference for both filled-cases went up by 20-30% in the visible region and 120-150% in the NIR region, following an inverse power law. This shows that the effects of wavelength specific absorption predominate over surface reflection. Phantom filled with standard refractive index fluid n1.33, and n1.46 should ideally show varying contrast as shown in the model results from Figure 4.7 flat, but the experimental results show a flat contrast. This is due to the absorption coefficient of the index fluids remaining constant across the visible and IR region while the coefficient of orange juice and ear fluids follows an inverse power law. Taken together, these results further the case for using NIR wavelengths for middle ear imaging and middle ear effusion diagnosis.

Following experimentation, we again ran the model to investigate the effects of differences in refractive indices, as a function of thin versus thick fluid, where indices range from 1.34 – 1.365 [27]. We ran the model to include fluids in the refractive index that range from n1.33, which corresponds to water, to n1.48, which is an arbitrarily high value that is much greater than

the refractive index of the back wall of the phantom. We assumed that the absorptions followed the power law curves calculated in Figure 3.4 for the TM and Figure 3.5 for the fluid. Furthermore, the model assumed a 10-degree angle of incidence, 500 um TM thickness and a 5mm thickness in the fluid area.

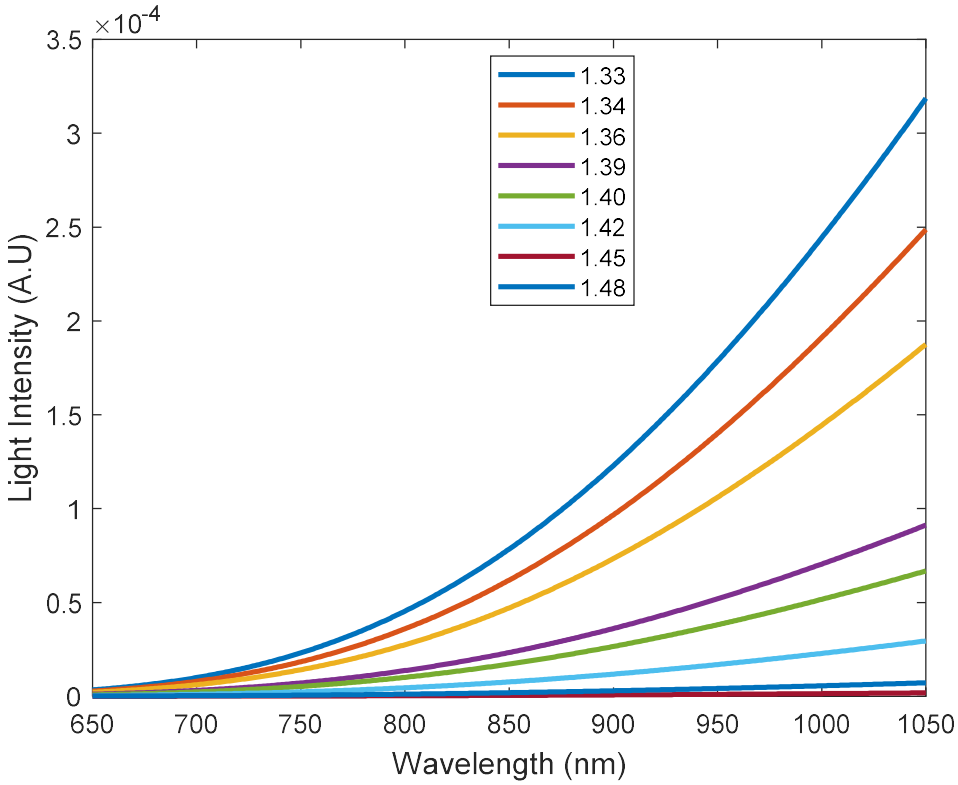

Figure 4.7 Reflectance Model output using fluids with different refractive indices

The results, shown in Figure 4.7, can be divided into three sections: The three highest refractive indices, 1.45, 1.48, 1.42 show a nearly flat response to changes in wavelengths, which we believe shows that refraction predominates due to "index mismatch" between the membrane and the fluid. Indices of 1.4 and 1.39 have a moderate response. Indices below that, namely 1.36,1.345 and 1.33, show a strong increase in intensity as a function of wavelength, which shows that absorption effects predominate. Orange juice has an index of 1.36 and this curve agrees with the results shown in Figure 4.5, where the contrast starts to change significantly only in the NIR region.

When comparing the intensity values of the model from the figure above, we find that the intensity value for fluid n1.39 at nIR (1000 nm) wavelength is same as that of intensity value

for fluid n1.36 at 850 nm. Now looking at the experimental results for orange juice (n1.36) as shown in Figure 4.5, we can find that the contrast values does not change significantly until 850 nm and the marginal increase in contrast from visible range (650 nm) is still within the uncertainty limits. Thus, by combing theoretical model and experimental results, we can argue that Vis-NIR multispectral imaging system might not be sensitive with fluids of refractive index 1.39 and higher.

The next question is how can the sensitivity of the system be increased? From the parameters that could contribute to variation, including detector quantum efficiency variation, source power variation, and the incident angle, we chose to model the incident angle, since the other parameters are already controlled through careful selection of components and calibration procedure.

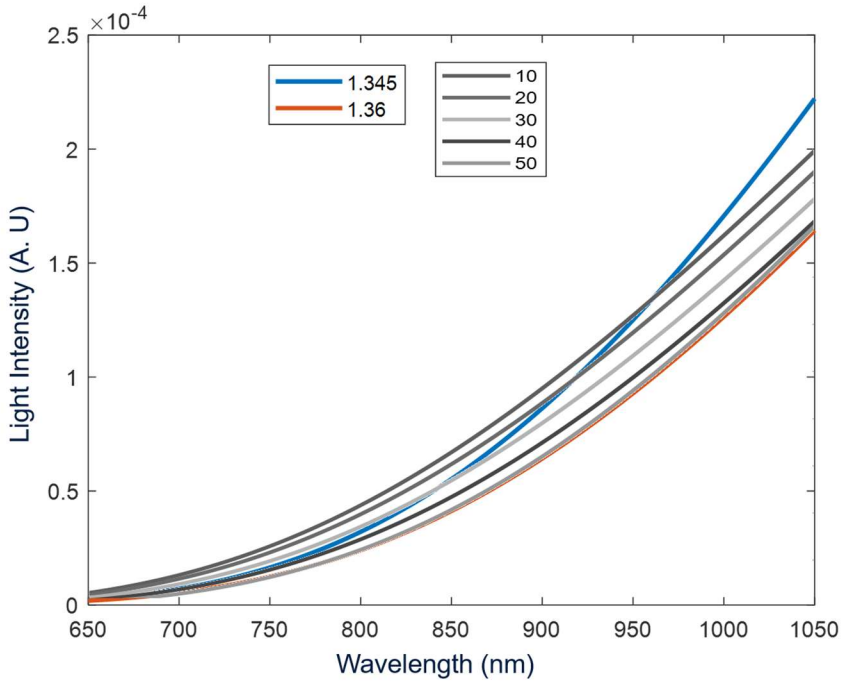

Figure 4.8 Reflection Model output for refractive index fluid of n1.36 at varying incident angles and n1.345 at 50°

The model was run for five different incident angles (in degrees) and the results are shown in Figure 4.8, for a refractive index of n1.36 and orange juice's absorption coefficient, with all other parameters are kept constant, including TM and fluid layer thicknesses. A single curve for n1.345 is also shown at a 50° incident angle. There are two key takeaways: 1) It can be clearly

seen that changing incident angles can affect the reflected output significantly, therefore, it is important to keep the incident angle stable during measurements so that the sensitivity of the system does not drop. 2) An incident angle change of 30° or more can play a significant role in resolving the fluid as the reflectance value changes with the angle. It is clearly seen that as the incident angle changes, the reflectance signal between the two different refractive index fluids starts overlapping in the nIR region. This could affect the ability to differentiate between serous fluid (OME) and thick mucous fluid (AOM). We aim to further deconstruct the effects of interference by performing a proof of concept study using an incoherent light source as explained in section 4.5.

4.4| Image Processing for fluid detection

In this section, we discuss the algorithm to detect and highlight the areas of the ear phantom filled with fluid by performing image analysis. This converts the numerical contrast data and presents the clinician with a qualitative, visual representation from which he or she can make a diagnosis. The flow chart in Figure 4.9 shows the image subtraction algorithm. Image subtraction, as a general technique, typically does not contribute significant noise, thus image fidelity is preserved.

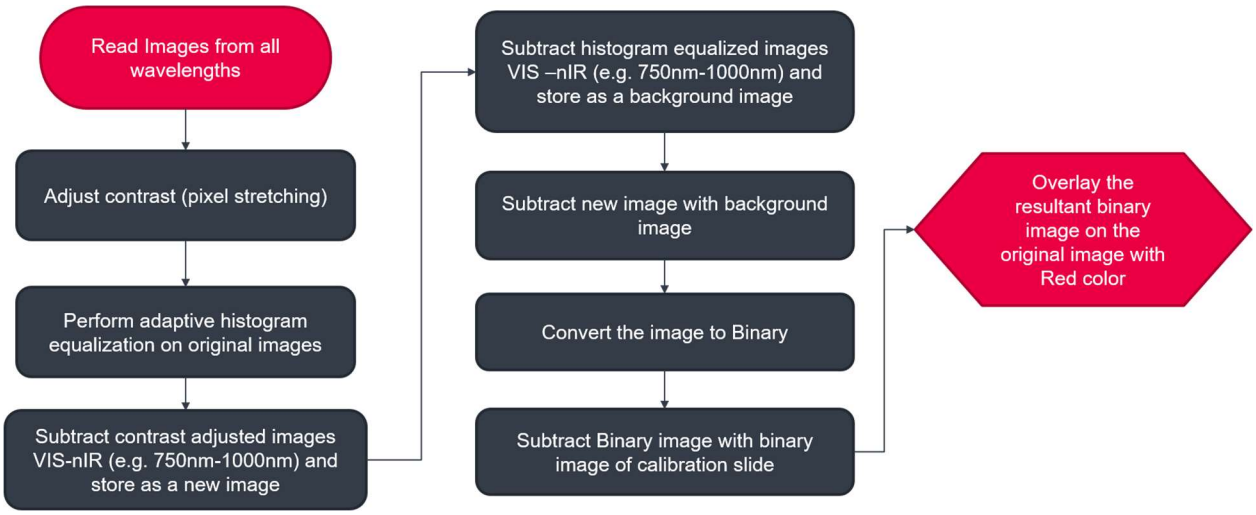

Figure 4.9 Flow chart of Image Processing algorithm to detect and highlight fluid in the acquired image

Taken step by step: The images are first acquired at two or more wavelengths. Since the images contain, highly reflective surfaces like bones, and absorbing surfaces like ear fluid, we use contrast adjustment to change the range of intensity values in the image from the standard 10-bit range (0 to 1023), to span the min and max intensities present in the image. This enhances the visual quality of the image and provide high contrast between bones (ossicles) and fluid. We then use adaptive histogram equalization to equalize intensity differences in smaller regions by computing many histograms and redistributing the intensity values. This helps to preserve the contrast difference between the bone, liquid and no-liquid areas of the phantom while providing minimal intensity variations in those areas, effectively smoothing the image.

The contrast adjusted images of Vis (650 nm – 800 nm) are subtracted from the NIR (900 nm – 1000 nm) images to detect the areas with fluid to contrast difference and create an image that only has fluid information. Similarly, the histogram equalized images of Vis and NIR wavelengths are also subtracted to create the background image. The background image is then subtracted from the fluid filled image to reduce the secondary reflection from bones, ossicles, etc. The subtracted image is then converted to a binary image which is then also subtracted with the binary image created from the calibration surface. This is done to reduce the interference effect from the source and any imperfections in the optics on the final output. This step is not shown in the flow chart and whether it is needed before each acquisition and how to implement it are open questions. The resultant binary image is then converted to read and overlaid on the visible light image. This way the augment image can be viewed with fluid filled areas highlighted.

The following series of images in Figure 4.10 shows the performance of the algorithm on various fluid levels. The rows show the image from visible and NIR wavelength and then the processed result, where the detected fluid is shown in color. The columns indicate various fluid levels from empty to full. The calibration images were taken with the Thorlabs reflective surface as discussed in section 4.1 before each trial and for each wavelength.

The 20%, 40% and 70% filled images show an increase in the red shaded areas as the fluid level increases. The empty image also has some highlighter regions, highlighted in blue. Despite calibration, this is due to the non-uniformity of the excitation signal. And by comparing to the red highlighted regions in the image this aberration is seen to repeat in all the images. Reducing this

is the subject of future work. It is clear that, overall, it would be very difficult to visually detect the fluid by examining the NIR and visible wavelength images alone, however, as the 20% filled case demonstrates, the proposed system is effective at detecting even small amounts of fluid. The figure below shows fluid detection using two wavelengths. We also expect a scenario where all the wavelengths presented in this experiment can also be incorporated to, potentially, provide more information or greater fidelity as each wavelength in itself can provide interesting information to physicians. This work is of future scope.

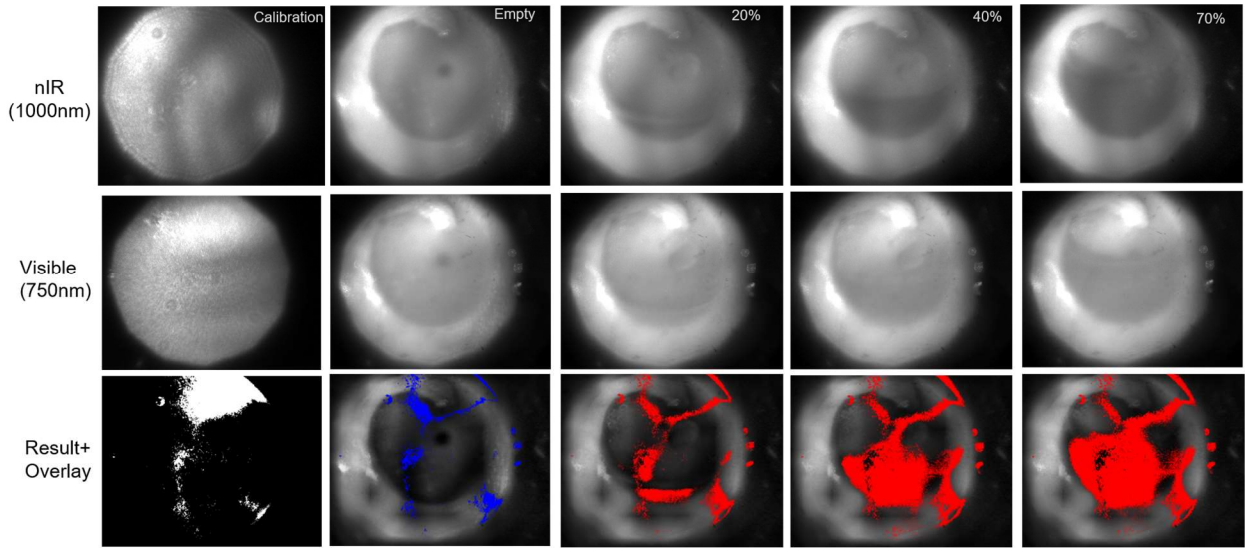

Figure 4.10 Results from image processing showing different levels of orange juice (~n1.36) fluid being detected and highlighted in red color.

4.5|Incoherent source (LED) imaging and analysis

The analysis from the previous subsections shows that the Vis – NIR multispectral imaging system is capable of detecting the fluid with high sensitivity in the ear phantom. Since we know the spectral response with empty and fluid-filled phantoms, the next step was to test the multispectral imaging concept with an incoherent source. Looking forward, this will address the cost issues, described in the system requirements in Chapter2, by enabling replacement of the laser source with LEDs. This would also be expected to address the interference patterns. The same setup, shown in Figure 3.9, calibration and data analysis protocols discussed were used, with the only change being the excitation source. Instead of a super-continuum laser source, we

used LEDs in the visible wavelength (660 nm, LED 660L, Thorlabs) and one in the nIR wavelength (910 nm, LED 910L, Thorlabs). These LEDs were readily available and the experiments are intended only as a proof of concept. This is not yet an optimized solution.

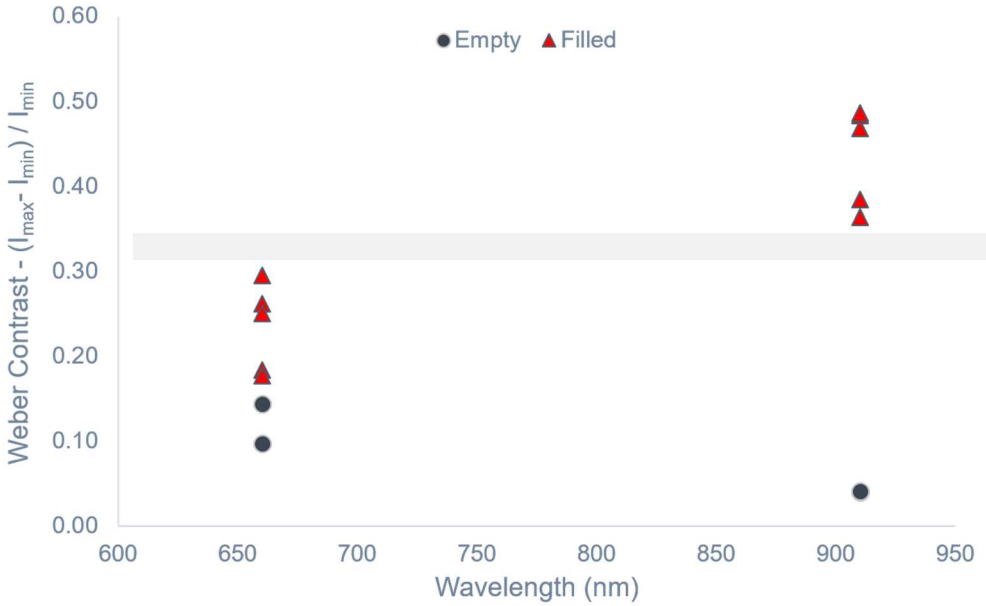

Figure 4.11 Contrast comparison on inter day samples between empty and filled phantoms imaged using an LED source at 660 nm and 910 nm

Figure 4.11 shows the contrast comparison between 660 nm and 910 nm for both the empty and fluid-filled case across multiple samples. Although a wavelength sweep was not possible, the contrast differences follow the same trend established earlier. The contrast value for coherent laser light source set-up increased by 35-40% between 660 nm and 900 nm for the liquid filled case and, by comparison, while the LED light source showed approximately a 50% difference in contrast, as shown in Figure 4.12. This increase in contrast over the laser source is due to the reduced variation due to the elimination of interference effects and represents a system improvement

This shows that conclusions drawn from the laser set-up are transferrable to an LED based system and that we have a means to reduce the cost and increase the sensitivity by moving. This was reiterated when we compared the intensities from the empty and liquid filled phantoms. Images at 660 nm shows only a marginal increase (1.2x - 2x) in contrast between the empty and filled case while the NIR (910 nm) shows a 3x – 4x increase in contrast, following the trend observed with the coherent sources.

The contrast graph in Figure 4.11 also shows uncertainty as high as 30-35% in absolute contrast between repetition of the same experiment on different days and 3-4% variation in contrast on the same day. The experiment is repeated three times on each day to test the validity of the results. One of the disadvantages of LEDs is that their optical power varies with an increase in junction temperature, therefore, their power can drift over time. One way to address this is by intermittent usage and proper thermal management when used for longer periods of time. Nevertheless, the LED system is still able to resolve the contrast between 660 nm and 910 nm for the given sample size.

Although by inspection there is a contrast difference between wavelengths, a two-tailed T-test was performed on all the samples, collected over from multiple days, for two means of unequal variance with a 95% confidence interval. The t-test indicated that the contrast difference between the filled images at 660 nm and 910 nm was not statistically significant. We believe this is due to the inter-day variation in LED intensity, which directly affects the absolute contrast values.

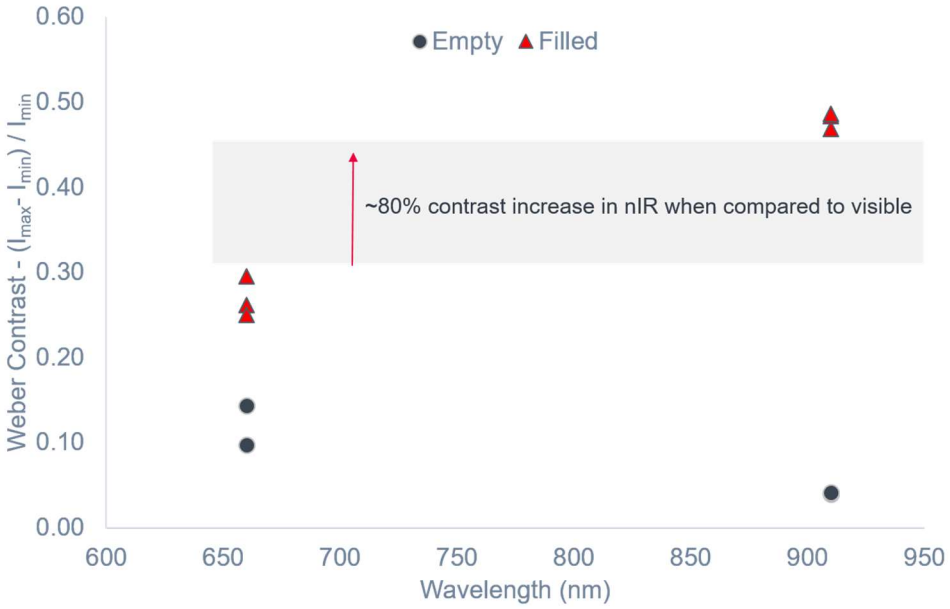

Figure 4.12 Contrast comparison on same day samples between empty and filled phantoms imaged using an LED source at 660 nm and 910 nm

This highlights the need for a calibration procedure on a more frequent basis when using LED sources, as their power varies with time. We have 3 data points from each day and, therefore, we tested just intra-day samples to find out if the LED-based system would be able to resolve the

empty and fluid cases. This t-test showed that the contrast difference between 660 nm and 910 nm for fluid filled case is statistically significant, with a contrast difference of 0.175 – 0.199 or an increase in contrast by 80%-95%, as shown in Figure 4.12. This contrast difference between Visible and NIR images can be greatly increased as we switch the NIR wavelength from 910 nm to 1000 nm to 1050 nm.

Figure 4.13 shows the qualitative images of empty and orange juice filled phantoms acquired using the LED source, for empty and 50%, 80% and 100% filled. We can see that the illumination is uniform and the interference effect is negligible. The same image processing algorithm was used and the contrast enhanced and subtracted images, shown in the last row, clearly indicate the presence of fluid. It is interesting to compare the empty and 100% filled case, which would be effectively indistinguishable with visible light (660 nm), since there is no change in contrast. Likewise, while the filled case in NIR (910 nm) shows higher contrast when compared to the empty case, it would be difficult to distinguish between the two without any baseline. Therefore, we conclude that using a multispectral imaging system with LED-based illumination we can compare the contrast between multiple wavelengths and use image processing techniques to detect fluid with high degree of sensitivity.

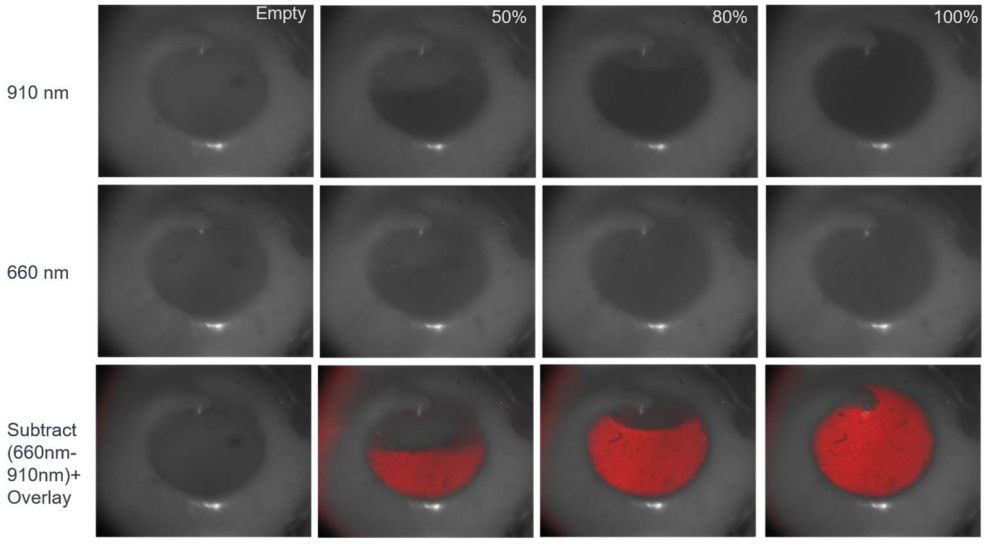

Figure 4.13 Results from LED imaging of the phantom showing different levels of orange juice liquid being detected and highlighted

Chapter 5 | Conclusion and Recommendation

The Vis – NIR (650 nm – 1050 nm) multispectral imaging system developed in this thesis can be the basis of a robust low-cost solution to detect the fluid in the middle ear. In this work, we provided a proof-of-concept of the system to show that we can detect the fluid with high sensitivity in middle ear phantoms. The multispectral imaging system exploits the difference in absorption, as a function of wavelength, between fluid filled and empty regions of the ear. Overall, reflectance in the fluid-filled areas is higher in the visible wavelength and decreases as we move towards the nIR region. Higher contrast for both empty and filled cases happens from 950 nm-1000 nm and we expect the trend to continue until 1100 nm based on the properties of ear fluid. Future work includes modelling to separate the effects of refraction from absorption, which will facilitate further sensitivity analysis.

Both Laser and LED sources were found to be effective in detecting the fluid due to the attenuation difference in the ear fluid and TM and both have pros and cons. While laser sources are stable, they have relatively high cost, sensitive to handle, and provide high variation and relatively low-quality visual results due to interference. LED sources are cheap, provide the same sensitivity as the laser system and high-quality visual results due to the absence of interference, however, they are less stable, as their power tend to vary over the time and with the prolonged use. Nevertheless, we recommend using LED sources control cost and continuously calibrate the output power. This could be accomplished by integrating a power meter or photodetector into the design.

Fluid-filled phantoms in NIR wavelengths (950 nm – 1000 nm) provided a 100 ± 20 % increase in contrast when compared to the visible wavelengths (650 – 800 nm). Calibration on a standard reflectance surface provides uniform intensity for empty images at all wavelengths, thus making it easier to detect the liquid when there is a change in contrast. The system can robustly resolve the difference between fluid and empty ear when the fluid in the middle ear has a refractive index in the range of 1.34 – 1.38. Further experiments are needed to ascertain if the system will be able to detect the difference in contrast for fluids of different refractive index vis-

à-vis thin serous fluid (OME) and thick mucous fluid (AOM). Additional work can be done to optimize the selected wavelengths.

The benchtop system is built on available standard optical and mechanical parts and therefore prototype miniaturization is needed before going for clinical studies. The prototype system can use single source and color filter for multispectral imaging to keep the size small. The key next steps are removing the system from the optical breadboard and compacting it into a system suitable for a human study.

References

All citations generated via the automated citation generation features of software package, Zotero (Version 5.0.80). Style guide used: IEEE.

1. "Https://www.Mayoclinic.Org/Diseases-Conditions/Ear-Infections/Symptoms-Causes/Syc-20351616," n.d.
2. A. S. Lieberthal *et al.*, "The Diagnosis and Management of Acute Otitis Media," *Pediatrics*, vol. 131, no. 3, p. e964, Mar. 2013, DOI: 10.1542/peds.2012-3488.
3. R. Kaur, M. Morris, and M. E. Pichichero, "Epidemiology of Acute Otitis Media in the Postpneumococcal Conjugate Vaccine Era.," *Pediatrics*, vol. 140, no. 3, Sep. 2017, DOI: 10.1542/peds.2017-0181.
4. S. Ahmed, N. L. Shapiro, and N. Bhattacharyya, "Incremental health care utilization and costs for acute otitis media in children.," *Laryngoscope*, vol. 124, no. 1, pp. 301–305, Jan. 2014, DOI: 10.1002/lary.24190.
5. https://www.reuters.com/article/us-health-antibiotics-pharma/pharma-firms-not-making-enough-progress-against-superbugs-report-idUSKBN1ZK1HQ.
6. https://photoni.care/history-of-the-otoscope
7. https://www.nasa.gov/pdf/458490main_TRL_Definitions.pdf.
8. J. A. Carr, T. A. Valdez, O. T. Bruns, and M. G. Bawendi, "Using the shortwave infrared to image middle ear pathologies," *Proc Natl Acad Sci USA*, vol. 113, no. 36, p. 9989, Sep. 2016, DOI: 10.1073/pnas.1610529113.
9. L. Hu *et al.*, "Towards an optical diagnostic system for otitis media using a combination of otoscopy and spectroscopy.," *J Biophotonics*, vol. 12, no. 6, p. e201800305, Jun. 2019, DOI: 10.1002/jbio.201800305.
10. N. Bedard, I. Tošić, L. Meng, and K. Berkner, "Light Field Otoscope," in *Imaging and Applied Optics 2014*, 2014, p. IM3C.6, DOI: 10.1364/ISA.2014.IM3C.6.
11. N. Bedard *et al.*, "Light field otoscope design for 3D in vivo imaging of the middle ear," *Biomed. Opt. Express*, vol. 8, no. 1, pp. 260–272, Jan. 2017, DOI: 10.1364/BOE.8.000260.
12. T. A. Valdez *et al.*, "Multi-color reflectance imaging of middle ear pathology in vivo," *Anal Bioanal Chem*, vol. 407, no. 12, pp. 3277–3283, May 2015, DOI: 10.1007/s00216-015-8580-y.
13. T. A. Valdez *et al.*, "Multiwavelength fluorescence otoscope for video-rate chemical imaging of middle ear pathology," *Anal Chem*, vol. 86, no. 20, pp. 10454–10460, Oct. 2014, DOI: 10.1021/ac5030232.
14. Anshuman J. Das, Julio C. Estrada, Zhifei Ge, Sara Dolcetti, Deborah Chen, and Ramesh Raskar, "A compact structured light based otoscope for three-dimensional imaging of the TM," presented at the Proc.SPIE, 2015, vol. 9303.
15. G. L. Monroy *et al.*, "Noninvasive depth-resolved optical measurements of the TM and middle ear for differentiating otitis media.," *Laryngoscope*, vol. 125, no. 8, pp. E276-282, Aug. 2015, DOI: 10.1002/lary.25141.

16. Z. Schmilovitch, V. Alchanatis, M. Shachar, and Y. Holdstein, “Spectrophotometric otoscope: A new tool in the diagnosis of otitis media,” *Journal of Near Infrared Spectroscopy - J NEAR INFRARED SPECTROSC*, vol. 15, Jan. 2007, DOI: 10.1255/jnirs.739.
17. Y. B. Ji *et al.*, “Terahertz otoscope and potential for diagnosing otitis media,” *Biomed Opt Express*, vol. 7, no. 4, pp. 1201–1209, Mar. 2016, DOI: 10.1364/BOE.7.001201.
18. J. Chan, S. Raju, R. Nandakumar, R. Bly, and S. Gollakota, “Detecting middle ear fluid using smartphones,” *Science Translational Medicine*, vol. 11, no. 492, p. eaav1102, May 2019, DOI: 10.1126/scitranslmed.aav1102.
19. Thiago Cavalcanti, Sewoong Kim, and Jae Youn Hwang, “Smartphone-based multispectral imaging otoscope for the diagnosis of otitis media (Conference Presentation),” presented at the Proc.SPIE, 2019, vol. 10881.
20. https://www.frequencytx.com/about-hearing-loss/.
21. M. Yu. Doladov, V. S. Kazakevich, I. G. Kalashnikov, V. V. Kupaeva, and V. A. Shcherbakov, “Optical Reflection Spectrum of the Human TM,” *Journal of Applied Spectroscopy*, vol. 68, no. 4, pp. 708–710, Jul. 2001, DOI: 10.1023/A:1012503029135.
22. C. Mignon, D. J. Tobin, M. Zeitouny, and N. E. Uzunbajakava, “Shedding light on the variability of optical skin properties: finding a path towards more accurate prediction of light propagation in human cutaneous compartments,” *Biomed Opt Express*, vol. 9, no. 2, pp. 852–872, Jan. 2018, DOI: 10.1364/BOE.9.000852.
23. G. Zonios and A. Dimou, “Light scattering spectroscopy of human skin in vivo,” *Opt. Express*, vol. 17, no. 3, pp. 1256–1267, Feb. 2009, DOI: 10.1364/OE.17.001256.
24. M. Hébert, L. Simonot, and S. Mazauric, “Matrix method to predict the spectral reflectance of stratified surfaces including thick layers and thin films,” May 2015.
25. L. Simonot, M. Hébert, and R. D. Hersch, “Extension of the Williams-Clapper model to stacked nondiffusing colored coatings with different refractive indices,” *J. Opt. Soc. Am. A*, vol. 23, no. 6, pp. 1432–1441, Jun. 2006, DOI: 10.1364/JOSAA.23.001432.
26. http://www.geocities.ws/dushang2000/Microscopy/Zeiss%20Refractometer%20Repair/Chem%202990%20Refractive%20Index%20Readings.pdf
27. E. N. Lazareva and V. V. Tuchin, “Blood refractive index modeling in the visible and near-infrared spectral regions,” Journal of Biomedical Photonics & Engineering; Vol 4, No 1 (2018): Laser and optical technologies in biomedicine and ecology - 10.18287/JBPE18.04.010503, Mar. 2018, [Online]. Available: http://jbpe.ssau.ru/index.php/JBPE/article/view/3278.
28. https://www.simtec-silicone.com/optical-liquid-silicone-rubber//
29. A. Argaw-Denboba, A. A. Abejew, and A. G. Mekonnen, “Antibiotic-Resistant Bacteria Are Major Threats of Otitis Media in Wollo Area, Northeastern Ethiopia: A Ten-Year Retrospective Analysis,” *Int J Microbiol*, vol. 2016, pp. 8724671–8724671, 2016, doi: 10.1155/2016/8724671.
30. M. E. Pichichero and M. D. Poole, “Assessing Diagnostic Accuracy and Tympanocentesis Skills in the Management of Otitis Media,” *Archives of Pediatrics*

& Adolescent Medicine, vol. 155, no. 10, pp. 1137–1142, Oct. 2001, doi: 10.1001/archpedi.155.10.1137.
31. P.-D. Sundvall, C. E. Papachristodoulou, and L. Nordeman, "Diagnostic methods for acute otitis media in 1 to 12 year old children: a cross sectional study in primary health care," *BMC Family Practice*, vol. 20, no. 1, p. 127, Sep. 2019, doi: 10.1186/s12875-019-1018-4.
32. E. Asher, E. Leibovitz, J. Press, D. Greenberg, N. Bilenko, and H. Reuveni, "Accuracy of acute otitis media diagnosis in community and hospital settings," *Acta Paediatrica*, vol. 94, no. 4, pp. 423–428, Apr. 2005, doi: 10.1111/j.1651-2227.2005.tb01912.x.
33. https://www.asha.org/public/hearing/Conductive-Hearing-Loss/.
34. https://www.cdc.gov/mmwr/preview/mmwrhtml/mm6019a2.htm?s_cid=mm6019a2_w.
35. "Optical Properties of Polylactides - Scientific Figure on ResearchGate. Available from: https://www.researchgate.net/figure/ndex-of-refraction-for-PLA-as-a-function-of-wavelength-from-a-global-determination-of-the_fig3_243974514."
36. https://www.mdedge.com/familymedicine/article/77660/air-fluid-levels-ear.
37. https://www.merckmanuals.com/home/ear,-nose,-and-throat-disorders/middle-ear-disorders/otitis-media-chronic-suppurative.
38. https://www.childrens.health.qld.gov.au/guideline-acute-otitis-media-emergency-management-in-children/.

[This page is intentionally left blank.]